syntrophin knockout mice (α1syn$^{-/-}$). In addition, we used nNOS knockout (nNOS$^{-/-}$) and eNOS knockout (eNOS$^{-/-}$) mice to clarify which NOS is involved in vasodilation under shear stress.

Materials and methods

Animals

Mdx mice and their controls, C57Bl/10 mice (B10), α1syn$^{-/-}$ mice generated in C57Bl/6 mice (B6), and their wild-type littermates (α1syn$^{+/+}$), aged 8-10 weeks were used (17). Eight- to 10-week-old nNOS$^{-/-}$ and eNOS$^{-/-}$ mice (B6 background) were supplied by the Jackson Laboratory. They were anesthetized by intraperitoneal injection of 1.2×10^{-3} g carbamic acid ethyl ester per gram of body weight. At the end of the experiment, animals were sacrificed by an overdose of pentobarbital. All protocols were approved by the Institutional Animal Care and Use Committee of the National Institute of Neuroscience and were performed in compliance with the Guide for the Care and Use of Division of Laboratory Animal Resources.

Experimental Design

We mounted and fixed mouse on experimental stage under anesthesia and scrotum of each mouse was placed on a clear silicone dish as shown in Figure 1a. The cremaster muscle was exposed as described with minor modification (18), and was observed under an intravital microscope at 450 magnifications. The exposed cremaster muscle was deoxygenated by continuous superfusion (5 ml/min) of buffered Tyrode solution (34 ± 0.5 °C, pH 7.35-7.45) bubbled with 95% N_2 and 5% CO_2 gas. Captured microcirculatory images were converted to digital images by the computer and recorded by VTR (Fig. 1a). To calculate the shear stress, we used CapiFlow® (IM-Capiflow, Kista, Sweden), a fully computerized system for the measurement of red blood cell velocity, as previously described (19, 20).

Drug treatment

We first examined the vasodilatory response of third-order arterioles (A3; about 20 μm) in mouse cremaster muscles (Fig. 1b) (22). ACh or SNP was added to the buffer solution and applied directly to the muscle, based on previous reports with modification (23, 24). The vessel diameter was measured before and just after drug administration and the dilatory ratio was calculated as: diameter of arteriole after drug treatment/ before drug treatment. To determine adequate dose, ACh or SNP was exposed from its lower concentration to higher concentration. Before increasing dose, we waited for maximum ten minutes until no more dilatory effect was observed by previous dose. Papaverin was added at the final part of experiments to know the extent of maximum dilation of vessels. We also examined the effect of NO synthesis inhibition by adding N-omega-nitro-L-arginine methyl ester (L-NAME, 0.1 mmol/L) to the buffer from 10 minutes before ACh or SNP administration.

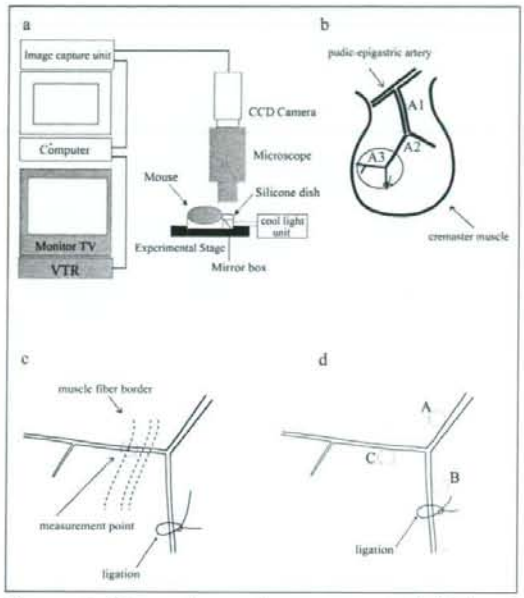

Figure 1. Observation and measurement of dilation of intramuscular arterioles induced by drug treatment or by shear stress in mouse cremaster muscle. (a) Optical system consisting of a cool light unit, mirror box, 450X intravital microscope (MZFL3, Leica Microsystems, Heidelberg, Germany), cooled, color 3 charge-coupled device (CCD) camera, image capture unit (C5810, Hamamatsu Photonics K.K., Hamamatsu, Japan), computer (Apple Macintosh G4, Apple, Cupertino, California), and video cassette recorder (HR-STG300, Victor JVC, Yokohama, JAPAN). (b) Arterioles in the mouse cremaster muscle are classified as indicated. A1; first-order arterioles, A2; second-order arterioles, A3; third-order arterioles. Observation area was indicated by circle. (c) Measurements of arteriole diameter were performed 120-1000 μm from the point of divergence, and the observation point was decided in reference to the border of muscle fibers. (d). Points for measurements of tissue pO_2 during parallel occlusion in A3 area: A, around the main arteriole; B, around the ligation site; and C, the original point for measurements of dilation of arterioles.

Shear stress

We used parallel occlusion method to increase the blood flow velocity in nonoccluded parallel arteriolar branches in vivo, based on the previous studies (13-16). The arteriole was ligated using 10-0 nylon thread with needle to produce shear stress (Fig. 1c) (13). The ligated portion and the measured point (A3) were remote enough from the branching point to avoid artifactual effects. The dilatory ratio for shear stress experiments was calculated as: diameter of arteriole after ligation/ before ligation. The dilatory ratio was also examined under indomethacin ($1.0x10^{-3}$, $5.0x10^{-2}$, $1.0x10^{-2}$ or 0.5 mmol/L) administration, when Prostaglandin I_2 (PGI_2) ($1.0x10^{-4}$ mmol/L) was added to the buffer solution or we induced vasodilation by parallel occlusion. L-NAME and indomethacin were supplied from 10 minutes before ligation. Without L-NAME treatment, shear stress-induced vasodilation was observed for a longer period as long as 20 minutes in 4 B10 and 4 *mdx* mice.

Measurements of partial pressure of oxygen (pO_2)

Observations of the microcirculation and in vivo partial pressure of oxygen (pO_2) measurements were made with a microscope and the oxygen-dependent quenching of phosphorescence decay technique, as previously described (21). We measured tissue pO_2 of B10 (n = 3) and *mdx* mice (n = 3) at three distinct points of cremaster muscles before and after ligation by the phosphorescence quenching method (Fig. 1d).

Histological analysis and immunohistochemistry

Ten-micrometer cryosections of cremaster muscles were prepared, air-dried, and stained with hematoxylin and eosin (H&E). Six-micrometer acetone-fixed cryosections were prepared, blocked with goat serum, and then incubated with primary antibodies, rabbit against nNOS (Zymed Laboratories) and rat against CD31/PECAM-1 (Southern Biotechnology Associates) at room air temperature. Alexa 488-labeled goat anti-rabbit IgG (H + L) (Molecular Probes) and Alexa 594-labeled goat anti-rat IgG (H + L) were used as the secondary antibody. The sections were viewed and photographed by a laser microscope, TCSSP™ (Leica Microsystems).

Statistical analysis

Results were expressed as means ± standard error of the mean (SEM). Results were compared between *mdx* mice and B10, α1syn$^{-/-}$ and α1syn$^{+/+}$ mice, and eNOS$^{-/-}$ or nNOS$^{-/-}$ mice and B6. The effect of L-NAME pretreatment was also evaluated. The significance of the differences between groups was determined by Mann-Whitney U test or ANOVA. Values of $p < 0.05$ were considered to be significant.

Results

Drug induced vasodilation

Maximum arteriolar dilation was determined for administration of ACh or SNP, and then compared with the dilation by the treatment with 1.0 mmol/L of Papaverine. The optimal dose of both ACh and SNP was 1.0 mmol/L for maximum dilatory ratio (Fig. 2) and the dose was used for subsequent examinations (Fig. 3).

The administration of ACh or SNP gave almost the same dilatory ratio between B10 (n = 7) and *mdx* mice (n = 7), α1syn$^{+/+}$ (n = 5) and α1syn$^{-/-}$ (n = 5) and, eNOS$^{-/-}$ (n = 4) or nNOS$^{-/-}$ mice (n = 4) and B6 (n = 4) (Figs. 3a and 3b). This result does not conflict with the conclusion of a previous study using nNOS- and eNOS-deficient mice that expression of either nNOS or eNOS is sufficient for ACh-induced dilation (25). Pretreatment of L-NAME gave the same degree of inhibition in ACh-induced vasodilation in B10 (n = 5) and in *mdx* mice (n = 5), but did not significantly alter the dilatory ratio in SNP-induced vasodilation in these mice.

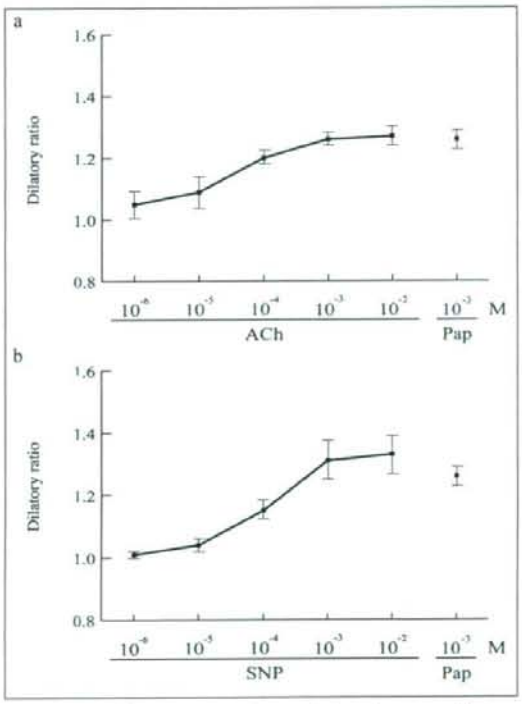

Figure 2. Responses of arterioles for vasodilatory agents, ACh and SNP in three B10. Graphs are showing dilatory ratio against various doses of ACh (a) or SNP (b), in reference to maximum dilation by treatment of 10^{-3} M of Papaverin (Pap).

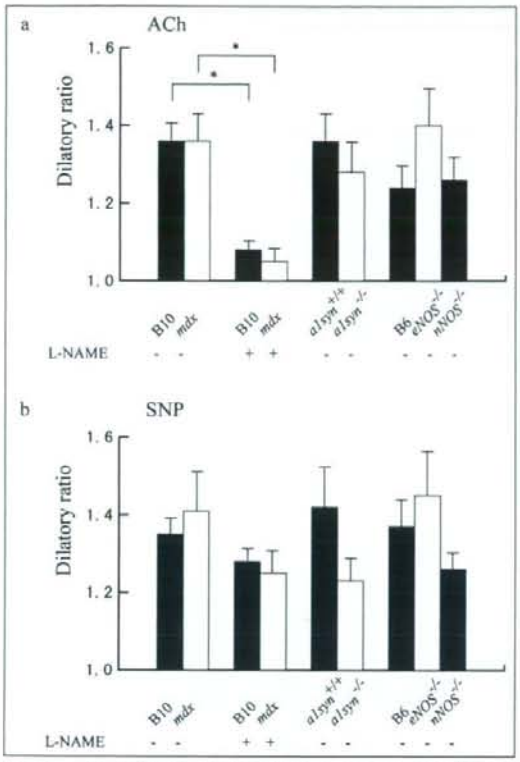

Figure 3. Effects of vasodilative agents on dilation of mouse cremaster arterioles of B10 (black bar), mdx (white bar), B10 pretreated with L-NAME (black bar), mdx pretreated with L-NAME (white bar), α1syn$^{+/+}$ (black bar), α1syn$^{-/-}$ (white bar), B6 (black bar), eNOS$^{-/-}$ (white bar), and nNOS$^{-/-}$ (black bar) mice. (a) After pretreatment with L-NAME, ACh-induced vasodilation was reduced both in B10 and in mdx mice. Values are indicated as mean ± SEM. Asterisk (*) shows statistical significance ($p < 0.05$). (b) Vasodilation induced by SNP was not statistically significant between the mice we examined.

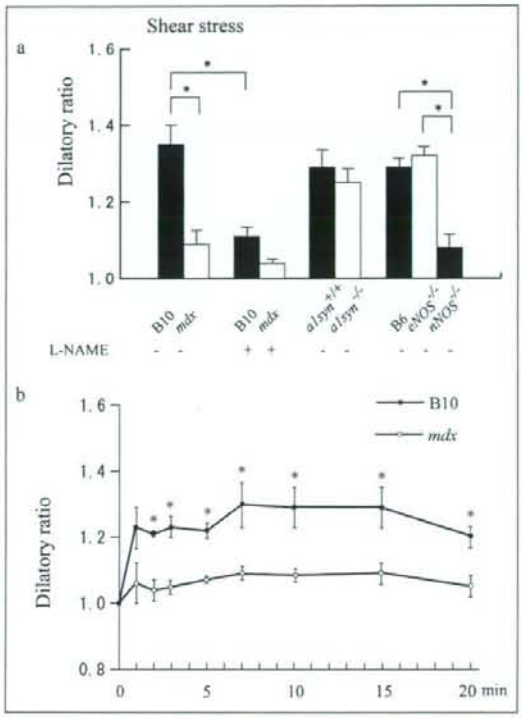

Figure 4. Effects of shear stress-induced dilation of mouse cremaster arterioles of B10 (black bar), mdx (white bar), B10 pretreated with L-NAME (black bar), mdx pretreated with L-NAME (white bar), α1syn$^{+/+}$ (black bar), α1syn$^{-/-}$ (white bar), B6 (black bar), eNOS$^{-/-}$ (white bar), and nNOS$^{-/-}$ (black bar) mice. (a) mdx mice, B10 pretreated with L-NAME, mdx mice pretreated with L-NAME and nNOS$^{-/-}$ mice showed impaired vasodilation under shear stress. (b) Extended observation of shear stress-induced vasodilation. The vessel diameter in B10 rapidly increased after vessel ligation and reached a stable level within 10 minutes (n = 4). The dilation of arterioles was severely impaired in mdx mice (n = 4). The difference between mdx mice and B10 was observed as long as 20 minutes after the ligation.

Shear stress-induced vasodilation

In contrast, shear stress-induced vasodilation was significantly impaired in *mdx* mice (n = 10) compared with that of B10 (n = 10) (Fig. 4a), and in addition, the calculated shear stresses were different (Table 1). Interestingly, although nNOS$^{-/-}$ mice (n = 5) showed impaired vasodilation, eNOS$^{-/-}$ mice (n = 5) did not show significant differences in the dilatory ratio when compared with that of B6 (n = 5), indicating that nNOS is the main supplier of NO in the shear stress-induced vasodilation of arterioles in skeletal muscle. On the other hand, α1syn$^{-/-}$ mice (n = 5) did not show significant differences in the dilation compared with the control α1syn$^{+/+}$ mice (n = 5), suggesting that the intramuscular localization of nNOS at the sarcolemma is not critical for shear stress-induced vasodilation. After pre-treatment with L-NAME, shear stress-induced vasodilation was significantly decreased in B10 (n = 5).

As shown in Figure 4b, under a longer observation of shear stress-induced vasodilation in the absence of L-NAME, the difference between *mdx* mice and B10 was still observed at least 20 minutes after the ligation.

Table 1. Relationship of vasodilation and shear stress in mouse cremaster arterioles.

	Blood cell velocity (cm/s)		Diameter (μm)		Shear stress rate
	before ligation	after ligation	before ligation	after ligation	
B10 (n = 3)	0.48 ± 0.05	0.67 ± 0.20	18.7 ± 0.9	24.2 ± 0.2	1.02 ± 0.16
mdx (n = 3)	0.41 ± 0.05	0.91 ± 0.23*	18.8 ± 0.7	19.8 ± 0.1*	2.02 ± 0.23*

Shear stress rates were calculated as (shear stress before ligation) / (shear stress after ligation). Values are expressed as mean ± S.E.M. * = $p < 0.05$

PGI_2 induced vasodilation

There were significant differences between shear stress-induced and PGI_2-induced vasodilation in dilatory ratios against high concentrations of indomethacin in B10 (Fig. 5). These data indicated that high concentration of indomethacin treatment could completely antagonize PGI_2-induced vasodilation, but the treatment cannot completely inhibit shear stress-induced vasodilation.

Alternation of pO_2 before and after ligation

There were no significant differences in tissue pO_2 levels between before and after ligation not only in B10 but also in *mdx* mice (Fig. 6).

Immunohistochemical observation of NOS expression

In H&E stained tissues, centrally nucleated fibers, which represent muscle regeneration, were observed in only *mdx* mice (Figs. 7a-e). The immunohistochemical analysis showed that nNOS was observed mainly at the sarcolemma rather than in the endothelium and vascular smooth muscle in B10 and $eNOS^{-/-}$ mice (Figs. 7b and 7h). In $\alpha 1syn^{-/-}$ mice, nNOS was not localized at the sarcolemma but remained in the cytoplasm (Fig. 7f), as previously reported (14, 26). Less nNOS was found in *mdx* mice, and it was not detected in $nNOS^{-/-}$ mice (Figs. 7d and 7j).

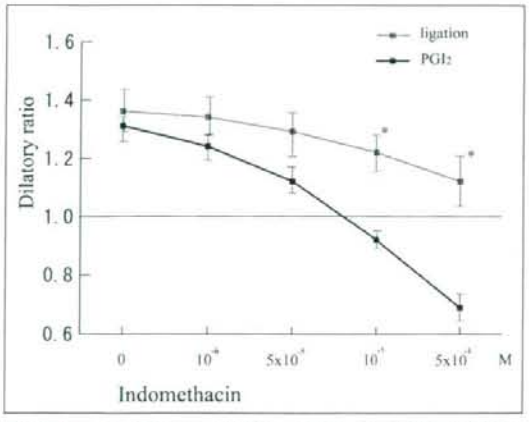

Figure 5. Under various dose of indomethacin, vasodilation was induced either by treatment of Prostaglandin I_2 (PGI_2) or by parallel occlusion (ligation) in B10 cremaster muscle arterioles (n = 5).

Discussion

Nitric oxide is one of the most important factors in shear stress-induced vasodilation especially by parallel occlusion method (10, 14, 27). Other factors, such as prostaglandins, were reported to contribute to shear stress-induced dilation in various models (15, 16, 28), but we showed that indomethacin, an inhibitor of prostaglandins, did not prevent the increase in diameter in shear stress condition. In addition, we concluded that the parallel occlusion method did not cause tissue hypoxia or acute ischemia. Thus, we demonstrated that dilation of arterioles in the mouse cremaster muscle under shear stress by the parallel occlusion method depends mainly on NO, especially that produced by nNOS. In particular, *mdx* and $nNOS^{-/-}$ mice showed impaired vasodilation in parallel occlusion,

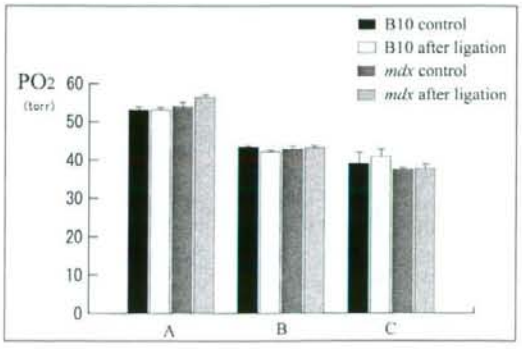

Figure 6. Histogram showing pO_2 at the observation points. There are no significant differences in alterations of tissue pO_2 during parallel occlusion.

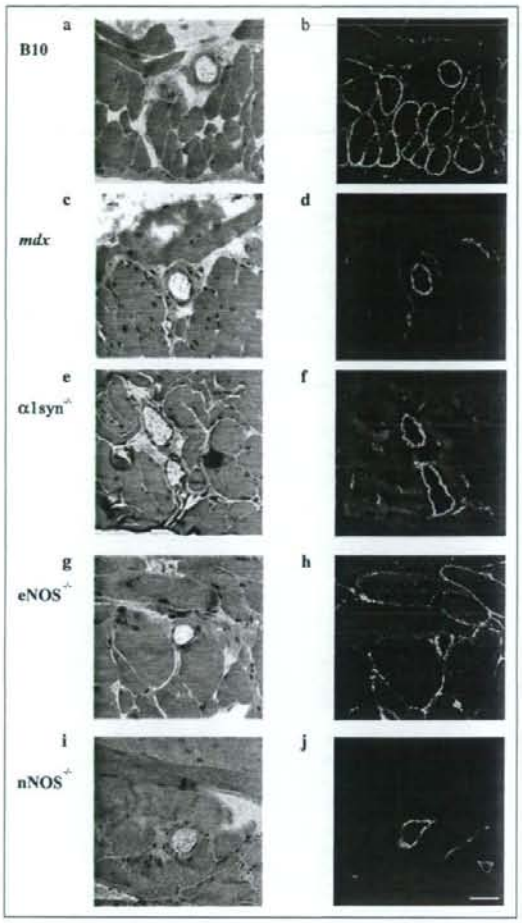

Figure 7. nNOS expression and localization in vascular endothelium and cremaster muscles of mice. H&E (a, c, e, g, and i) and double staining with nNOS (green) and PECAM-1 (red) antibodies (b, d, f, h, and i) of B10 (a, b), mdx (c, d), α1syn$^{-/-}$ (e, f), eNOS$^{-/-}$ (g, h), and nNOS$^{-/-}$ (i, j) mice. Centrally located nuclei, a typical feature of regenerated muscle, are found only in mdx mice (c). In B10 and eNOS$^{-/-}$ cremaster muscles, nNOS expression was observed at the sarcolemma. In contrast, the expression was greatly reduced or not detected in mdx or nNOS$^{-/-}$ mice, respectively. Bar, 40 μm.

whereas responses to ACh and SNP were unaltered. Decreased expression of nNOS in *mdx* skeletal muscle may be important as a cause of this finding.

It is intriguing to know the relationship between shear stress-induced vasodilation and the localization of nNOS. Koller et al. showed that shear stress-induced vasodilation of 80- to 156-μm arterioles was inhibited by removal of the endothelium or by addition of indomethacin in rat cremaster muscle, but they did not identify the responsible molecules of vascular dilation (29). In our study, nNOS expression was mainly found in the sarcolemma and less frequently in the endothelium or vascular smooth muscle, implying that skeletal muscle nNOS is possibly involved in dilation of intramuscular arterioles at the very end of the skeletal muscle circulation under shear stress. nNOS is anchored to the sarcolemma through α1-syntrophin. α1syn$^{-/-}$ mice showed altered distribution of nNOS expression in cytoplasm, but showed no significant differences in shear stress-induced vasodilation between α1syn$^{-/-}$ mice and α1syn$^{+/+}$ mice. Thus, the sarcolemmal localization of nNOS through expression of α1-syntrophin is not indispensable for vasodilation. However, how dystrophin or other molecules transduce mechanostress to soluble nNOS is unresolved (6). The defective vasodilation under shear stress due to nNOS deficiency in *mdx* mice might be related to its muscle degradation (14).

It is very interesting to note the amelioration of dystrophic phenotypes in nNOS transgenic *mdx* mice, although the localization of nNOS cannot have been improved (30). Decreased vasodilation just after muscle contraction has also been demonstrated in *mdx* skeletal muscle (31). Leinonen et al. found that capillary circulation in skeletal muscle was impaired in DMD (32), and deteriorated attenuation of α-adrenergic vasoconstriction during exercise may participate in this pathophysiology (7). Moreover, blood flow must be increased to accommodate the augmented metabolic demands of the muscle, not only in exercise. Intramuscular arterioles in *mdx* mice cannot afford to respond to the increased demands, and their failure may result in relative ischemia in the skeletal muscle and cardiac phenotypes of dystrophin deficiency. Asai et al. very recently showed that the functional ischemia in contraction-induced myofibers in *mdx* mice is due to nNOS deficiency and indicated that vasoactive drugs may ameliorate muscle damage (33). Even in dystrophin-deficient skeletal muscle, cholinergic vascular modulation was well preserved. Therefore, our study indicates that pharmacological treatment using a vasoactive agent is applicable to at least skeletal muscle symptoms in patients suffering from DMD.

In conclusion, we demonstrated that vasodilation of intramuscular arterioles under shear stress was impaired in dystrophin-deficient *mdx* mice. This impairment may be related to phenotypes of DMD, not only in skeletal muscle but also in cardiac muscle.

Acknowledgements

This work was supported by Grants-in-Aid from the Human Frontier Science Program, Scientific Research for

Center of Excellence, Research on Nervous and Mental Disorders (10B-1, 13B-1), Health Science Research Grants for Research on the Human Genome and Gene Therapy (H10-genome-015, H13-genome-001) and for Research on Brain Science (H12-brain-028) from the Ministry of Health, Labor, and Welfare of Japan, Grants-in-Aid for Scientific Research (10557065, 11470153, 11170264, 14657158, and 15390281) from the Ministry of Education, Culture, Sports, Science, and Technology for Japan, and a Research Grant from the Human Frontier Science Project. This work was also carried out as a part of the "Ground-based Research Announcement for Space Utilization" promoted by the Japan Space Forum. T. Yokota is a Research Fellow of the Japan Society for the Promotion of Science (JSPS).

References

1. Brenman JE, Chao DS, Xia H, et al. Nitric oxide synthase complexed with dystrophin and absent from skeletal muscle sarcolemma in Duchenne muscular dystrophy. Cell 1995;82:743-52.
2. Chang W, Iannaccone ST, Lau KS, et al. Neuronal nitric oxide synthase and dystrophin-deficient muscular dystrophy. Proc Nat Acad Sci USA 1996;93:9142-7.
3. Brenman JE, Chao DS, Gee SH, et al. Interaction of nitric oxide synthase with the postsynaptic density protein PSD-95 and α1-syntrophin mediated by PDZ domains. Cell 1996;84:757-67.
4. Yokota T, Miyagoe Y, Hosaka Y, et al. Aquaporin-4 is absent at the sarcolemma and at perivascular astrocyte endfeet in α1-syntrophin knockout mice. Proc Japan Acad 2000;76B:22-7.
5. Hoffman EP, Brown RH Jr, Kunkel LM. Dystrophin: the protein product of the Duchenne muscular dystrophy locus. Cell 1987;51:919-28.
6. Suzuki N, Motohashi N, Uezumi A, et al. NO production results in suspension induced muscle atrophy through dislocation of neuronal NOS. J Clin Invest 2007;117:2468-76.
7. Thomas GD, Sander M, Lau KS, et al. Impaired metabolic modulation of α-adrenergic vasoconstriction in dystrophin-deficient skeletal muscle. Proc Natl Acad Sci USA 1998;95:15090-5.
8. Fadel PJ, Zhao W, Thomas GD. Impaired vasomodulation is associated with reduced neuronal nitric oxide synthase in skeletal muscle of ovariectomized rats. J Physiol 2003;549:243-53.
9. Thomas GD, Shaul PW, Yuhanna IS, et al. Vasomodulation by skeletal muscle-derived nitric oxide requires α-syntrophin-mediated sarcolemmal localization of neuronal nitric oxide synthase. Circ Res 2003;92:554-60.
10. Loufrani L, Matrougui K, Gorny D, et al. Flow (shear stress)-induced endothelium-dependent dilation is altered in mice lacking the gene encoding for dystrophin. Circulation 2001;103:864-70.
11. Loufrani L, Li Z, Levy BI, et al. Excessive microvascular adaptation to chronic changes in blood flow in mice lacking the gene encoding for desmin. Arterioscler Thromb Vasc Biol 2002;22:1579-84.
12. Loufrani L, Henrion D. Vasodilator treatment with hydralazine increases blood flow in *mdx* mice resistance arteries without vascular wall remodeling or endothelium function improvement. J Hyperten 2005;23:1855-60.
13. Koller A, Kaley G. Flow velocity-dependent regulation of microvascular resistance in vivo. Microcirc Endothelium Lymphatics 1989;6:519-29.
14. Koller A, Kaley G. Endothelium regulates skeletal muscle microcirculation by a blood flow velocity-sensing mechanism. Am J Physiol 1990;258:H862-8.
15. Koller A, Kaley G. Prostaglandins mediate arteriolar dilation to increased blood flow velocity in skeletal muscle microcirculation. Circ Res 1990;67:529-34.
16. Frisbee JC, Stepp DW. Impaired NO-dependent dilation of skeletal muscle arterioles in hypertensive diabetic obese Zucker rats. Am J Physio. Heart Circ Physiol 2001;281:H1304-11.
17. Kameya S, Miyagoe Y, Nonaka I, et al. α1-Syntrophin gene disruption results in the absence of neuronal-type nitric-oxide synthase at the sarcolemma but does not induce muscle degeneration. J Biol Chem 1999;274:2193-200.
18. Baez S. An open cremaster muscle preparation for the study of blood vessels in vivo. Microscopy Microvasc Res 1973;5:384-94.
19. Fagrell B, Rosen L, Eriksson SE. Computerized data analysis of capillary blood cell velocity in humans. Int J Microcirc Clin Exp 1994;14:133-8.
20. Bongard O, Fagrell B. Discrepancies between total and nutritional skin microcirculation in patients with peripheral arterial occlusive disease (PAOD). Vasa 1999;19:105-11.
21. Shibata M, Ichioka S, Ando J, et al. Microvascular and interstitial PO(2) measurements in rat skeletal muscle by phosphorescence quenching. Appl Physiol 2001;91:321-7.
22. Kaul DK, Fabry ME, Costantini F, et al. In vivo demonstration of red cell-endothelial interaction, sickling and altered microvascular response to oxygen in the sickle transgenic mouse. J Clin Invest 1995;96:2845-53.
23. Ichioka S, Shibata M, Kosaki K, et al. Effects of shear stress on wound-healing angiogenesis in the rabbit ear chamber. J Surg Res 1997;72:29-35.
24. Ichioka S, Nakatsuka T, Ohura N, et al. Topical application of amrinone (a selective phosphodiesterase III inhibitor) for relief of vasospasm. J Surg Res 2000;93:149-55.
25. Meng W, Ayala C, Waeber C, et al. Neuronal NOS-cGMP-dependent ACh-induced relaxation in pial arterioles of endothelial NOS knockout mice. Am J Physiol 1998;274:H411-5.
26. Miyagoe-Suzuki Y, Takeda S. Association of neuronal nitric oxide synthase (nNOS) with α1-syntrophin at the sarcolemma. Microsc Res Tech 2001;55:164-70.
27. Boegehold MA. Flow-dependent arteriolar dilation in normotensive rats fed low- or high-salt diets. Am J Physiol 1995;269:H1407-14.
28. Sun D, Huang A, Smith CJ, et al. Enhancing release of prostaglandins contributes to flow-induced arteriolar dilation in eNOS knockout mice. Circ Res 1999;85:288-93.
29. Koller A, Sun D, Kaley G. Role of shear stress and endothelial prostaglandins in flow- and viscosity-induced dilation of arterioles in vitro. Circ Res 1993;72:1276-84.
30. Wehling M, Spencer MJ, Tidball JG. A nitric oxide synthase transgene ameliorates muscular dystrophy in *mdx* mice. J Cell Biol 2001;155:123-31.
31. Lau KS, Grange RW, Chang WJ, et al. Skeletal muscle contractions stimulate cGMP formation and attenuate vascular smooth muscle myosin phosphorylation via nitric oxide. FEBS Lett 1998;431:71-4.
32. Leinonen H, Juntunen J, Somer H, et al. Capillary circulation and morphology in Duchenne muscular dystrophy. Eur Neurol 1979;18:H714-21.
33. Asai A, Sahani N, Kaneki M, et al. Primary role of functional ischemia, quantitative evidence for the two-hit mechanism, and phosphodiesterase-5 inhibitor therapy in mouse muscular dystrophy. PLoS ONE 2007;29:e806.

OPEN ACCESS Freely available online

PLoS one

Activin in the Brain Modulates Anxiety-Related Behavior and Adult Neurogenesis

Hiroshi Ageta[1,2], Akiko Murayama[1,2], Rika Migishima[1], Satoshi Kida[2,4], Kunihiro Tsuchida[5], Minesuke Yokoyama[1,6], Kaoru Inokuchi[1,2,3]*

1 Mitsubishi Kagaku Institute of Life Sciences (MITILS), Machida, Tokyo, Japan, **2** Japan Science and Technology Corporation (JST), CREST, Kawaguchi, Japan, **3** Graduate School of Environment and Information Sciences, Yokohama National University, Yokohama, Japan, **4** Department of Bioscience, Tokyo University of Agriculture, Setagaya-ku, Tokyo, Japan, **5** Division for Therapies Against Intractable Diseases, Institute for Comprehensive Medical Science, Fujita Health University, Aichi, Japan, **6** Brain Research Institute, Niigata University, Niigata, Japan

Abstract

Activin, a member of the transforming growth factor-β superfamily, is an endocrine hormone that regulates differentiation and proliferation of a wide variety of cells. In the brain, activin protects neurons from ischemic damage. In this study, we demonstrate that activin modulates anxiety-related behavior by analyzing ACM4 and FSM transgenic mice in which activin and follistatin (which antagonizes the activin signal), respectively, were overexpressed in a forebrain-specific manner under the control of the αCaMKII promoter. Behavioral analyses revealed that FSM mice exhibited enhanced anxiety compared to wild-type littermates, while ACM4 mice showed reduced anxiety. Importantly, survival of newly formed neurons in the subgranular zone of adult hippocampus was significantly decreased in FSM mice, which was partially rescued in ACM4/FSM double transgenic mice. Our findings demonstrate that the level of activin in the adult brain bi-directionally influences anxiety-related behavior. These results further suggest that decreases in postnatal neurogenesis caused by activin inhibition affect an anxiety-related behavior in adulthood. Activin and its signaling pathway may represent novel therapeutic targets for anxiety disorder as well as ischemic brain injury.

Citation: Ageta H, Murayama A, Migishima R, Kida S, Tsuchida K, et al. (2008) Activin in the Brain Modulates Anxiety-Related Behavior and Adult Neurogenesis. PLoS ONE 3(4): e1869. doi:10.1371/journal.pone.0001869

Editor: Seth G. N. Grant, Wellcome Trust Sanger Institute, United Kingdom

Received August 24, 2007; **Accepted** February 22, 2008; **Published** April 2, 2008

Funding: This work was supported by the Special Coordinate Funds for Promoting Science and Technology from MEXT of the Japanese Government (K.I.), and in part by a Grant-in-Aid for Scientific Research on Priority Areas "Neural Circuit Project", "Advanced Brain Science Project", and "Molecular Brain Science", from MEXT of the Japanese Government (K.I.).

Competing Interests: The authors have declared that no competing interests exist.

* E-mail: kaoru@mitils.jp

Introduction

Anxiety disorder represents one of the most common mental illnesses [1–3]. Recently, disturbance in adult hippocampal neurogenesis was proposed to underlie anxiety-like behavior in rodents [4,5]; however, molecular mechanisms that link hippocampal neurogenesis to anxiety disorder remains poorly understood.

Activin, a member of the transforming growth factor-β superfamily, is an endocrine hormone that regulates differentiation and proliferation of a wide variety of cells [6]. In the brain, activin receptor ActRII is highly expressed in forebrain region [7,8], and its scaffold protein ARIP/S-SCAM is also localized in synaptic region [9,10]. Furthermore, activin protects neurons from ischemic damage [11], and its expression is upregulated by neuronal activity [12,13]. Recently, we showed that activin modulates dendritic spin morphology that is important for synaptic plasticity in the hippocampus [14,15].

In this study, we generated and analyzed transgenic mice in which activin function in the forebrain is either suppressed or enhanced. We found that the activin activity in the adult forebrain influences locomotor activity, anxiety-related behavior, and hippocampal neurogenesis.

Results

We explored the role activin plays in anxiety-related behavior using a transgenic mouse model that overexpresses activin or follistatin, an activin-inhibitory protein, in a forebrain-specific manner. Disturbance of activin signal during the developmental stage causes a lethal phenotype in mammals [16,17]. To achieve postnatal, forebrain-specific expression, the αCaMKII promoter was used to drive expression of a transgene (**Fig. 1A**) [18,19]. We microinjected activin and follistatin transgenes into 549 and 1183 fertilized eggs, and obtained 42 and 55 weaned mice, respectively. From these, two lines of activin transgene-integrated mice (designated ACM3 and ACM4) and one line of follistatin transgene-integrated mice (designated FSM) were obtained. Transgene-integrated mice were generated in 1% of microinjected fertilized eggs [20]. This low efficacy may have been caused by unexpected transgene expression in various tissues during the embryonic stage, because the activin signal is important for normal development. In contrast to previously generated activin- or follistatin-transgenic mice [21–23], these heterozygous transgenic mice were fertile and bred healthily, and their body weight (data not shown) and muscular strength were normal when compared to their wild-type littermates (**Figure S1**). Since ACM3 mice showed

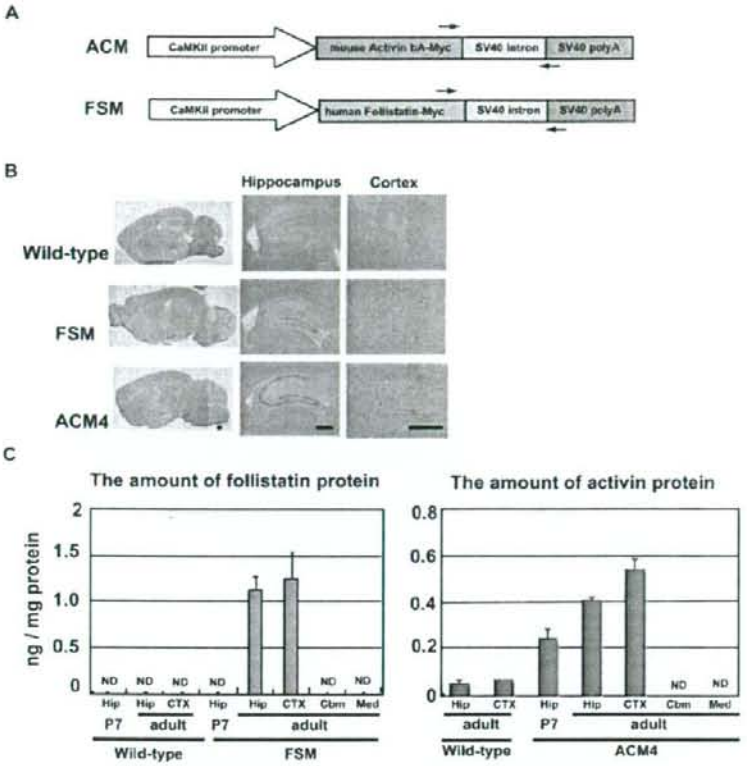

Figure 1. Generation of transgenic mice and expression analysis of the transgene. (A) Schematic representation of transgene constructs. Narrow arrows indicate the location and direction of RT-PCR primers (**Figure S2**). (B) Photographs of typical *in situ* hybridization are shown. DIG-labeled cRNA probe corresponding to the SV40 polyA sequence was hybridized to sagittal sections of the brain from 16–22 week-old wild-type, FSM and ACM4 mice. Scale bars, 500 μm. (C) Follistatin and activin protein levels in the hippocampus (Hip), cortex (CTX), cerebellum (Cbm) and medulla (Med) in wild-type, FSM and ACM4 mice measured by ELISA. Results are shown as mean ± s. e. m. (n = 4) Except for activin in CTX in wild-type (n = 1). Adult indicates 16–22 weeks-old. P7, postnatal day 7.
doi:10.1371/journal.pone.0001869.g001

phenotypes similar to ACM4 mice in behavioral experiments, we hereafter describe the phenotypes of ACM4 and FSM mice.

In situ hybridization analyses of brain sections revealed that transgene expression was restricted to the forebrain such as the hippocampus and neocortex in the adult brain (**Fig. 1B**). ELISA analyses also showed forebrain-specific expression of activin and follistatin in ACM4 and FSM adult mice, respectively (**Fig. 1C**). Low level of endogenous activin was detected in the hippocampus and neocortex in wild-type mice. Follistatin level in FSM was enough to antagonize this level of activin activity [24]. Follistatin was not detected in the infant hippocampus of FSM mice (**Fig. 1C**). RT-PCR revealed that follistatin- and activin-transgene were not expressed in peripheral tissues including, heart, lung, spleen, liver and kidney (**Figure S2**). Nissel staining showed no apparent structural abnormality in the hippocampus of each transgenic mice (**Figure S3**).

Open field tests were performed on transgenic mice to investigate locomotor activity (**Fig. 2**). FSM mice showed a decrease in time spent in locomotion and rearing when compared with wild-type littermates. In contrast, ACM4 mice showed a significant increase in rearing time. There was no genotype effect in the walking speed (**Fig. 2B**) and the total pathlength (**Fig. 2C**), indicating that walking ability of FSM and ACM4 mice was normal. These results indicate that the level of functional activin in the brain is related to general locomotor activity in a novel environment.

In open field tests, the amount of time spent in the center of the field is strongly correlated with an animal's level of anxiety, a characteristic called risk-taking behavior [25,26]. FSM mice showed decreased performance in risk-taking behavior (**Fig. 2D**), while ACM4 mice showed increased performance. To further assess these differences, a light and dark choice test and elevated plus-maze test were conducted. In the light and dark test, ACM4 mice accessed the lighted compartment significantly more often than wild-type littermates (**Fig. 3A**), however, FSM mice spent significantly more time in the dark compartment as compared to wild-type littermates. In the elevated plus-maze test, ACM4 mice spent significantly more time in the open arms of the testing apparatus than did wild-type and FSM mice (**Fig. 3B**). FSM mice showed no significant change in phenotype for this test.

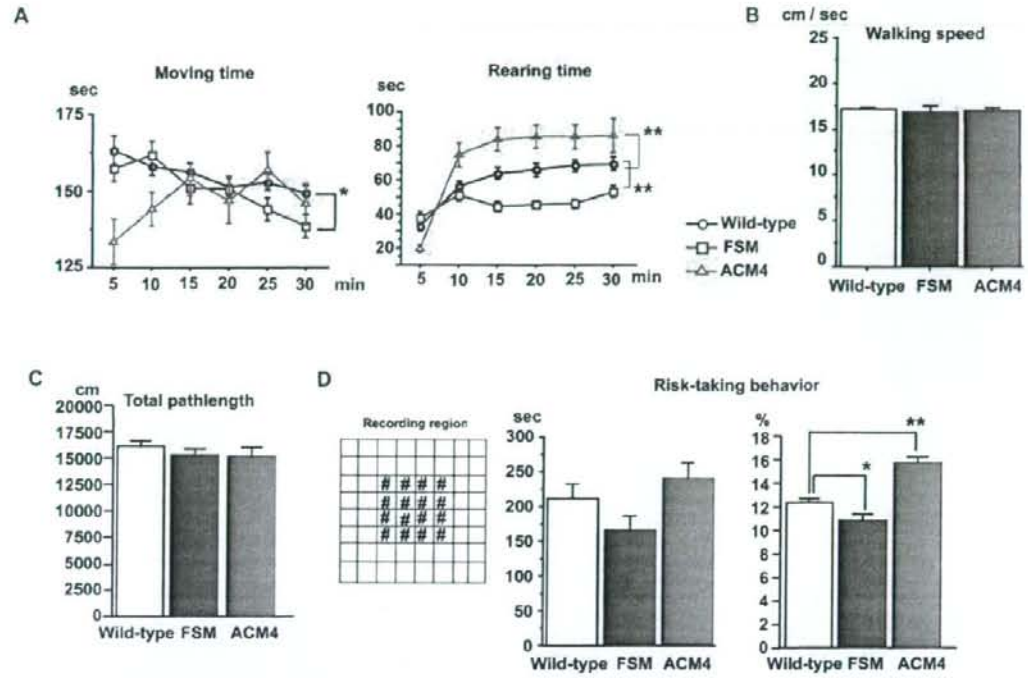

Figure 2. Activin protein levels in the brain influence locomotor activity. (A) Statistical analyses of the open field test showing time spent in locomotion and rearing [wild-type littermates (black circles), n = 34; FSM (blue squares), n = 18; ACM4 (red triangles), n = 11]. Each plot represents an average of 5 minutes. *, $p<0.05$; **, $p<0.001$; Fisher's test. (B and C) Statistical analyses of walking velocity (B) and total pathlength (C) during 30 minutes of open field test. (D) Risk taking behavior test. Left panel, overhead view of the box used for open field test. #, area defined as a center region. Mid panel, time spent in the center region during the 30 minutes of open field testing. Right panel, the percentage pathlength in the center region. Results are shown as mean ± s. e. m.
doi:10.1371/journal.pone.0001869.g002

We next designed and performed an original behavioral test to measure anxiety levels (**Fig. 3C**), based on the observation that mice generally prefer novel objects encountered in a familiar place [27]. In this test, mice were placed in a closed box on the first day to become familiar with the box. On the second day mice were placed in the same box to which a cylinder with two entrances (novel area) had been added. FSM mice spent significantly less time accessing the novel area as compared to wild-type mice, while the total distance they traveled during the test was normal. This suggests that higher anxiety in FSM mice resulted in lower access to the novel area. Taken together, the level of functional activin in the brain modulates anxiety-related behavior. Finally, no depressive behavior was observed in FSM mice in the forced swimming test (**Figure S4**).

Adult neurogenesis is the production of new neurons in areas of the adult brain including the subventricular zone (SVZ) and subgranular zone (SGZ) of the hippocampus [28]. This formation of new neurons plays a number of physiological roles including damaged neuron replacement[29,30], memory formation [31,32] and response to stress [33]. Moreover, some reports have recently shown that neurogenesis is involved in depression [34,35].

We therefore examined adult neurogenesis in hippocampal SGZ of FSM and ACM4 mice (**Fig. 4**) using 5-bromodeoxyuridine (BrdU)-labeling experiments. Transgenic mice were injected with BrdU (75 mg/kg body weight) three times per day for three consecutive days. Mice were sacrificed either 24 h or 4 weeks after the final injection day. BrdU is incorporated into genomic DNA by cells at S-phase, therefore, by staining with a neuronal marker (NeuN) and an anti-BrdU antibody, newly generated neurons were easily detected. A significant difference between FSM and ACM4 mice was observed in the number of SGZ BrdU-positive cells after 24 h (**Fig. 4A, B**). No significant difference, however, was observed between transgenic mice and wild-type littermates, indicating that the number of neuronal progenitor cells and the rate of BrdU incorporation into progenitor cells in transgenic mice were essentially normal. At the 4-week stage, however, the number of BrdU- and NeuN-double positive cells in FSM mice was markedly decreased (**Fig. 4C**). This reduction was partially rescued by crossing with ACM4 (**Fig. 4D**). These results indicated that the level of activin in the brain is crucial for the maturation and maintenance of newly generated neurons.

The decrease in BrdU- and NeuN-double positive cells at the 4-week stage may be attributed to a decrease in the survival rate of newly formed neurons or a decrease in the rate for neuronal differentiation of new cells. Therefore, the change in the number of BrdU- and NeuN-double positive cells following BrdU

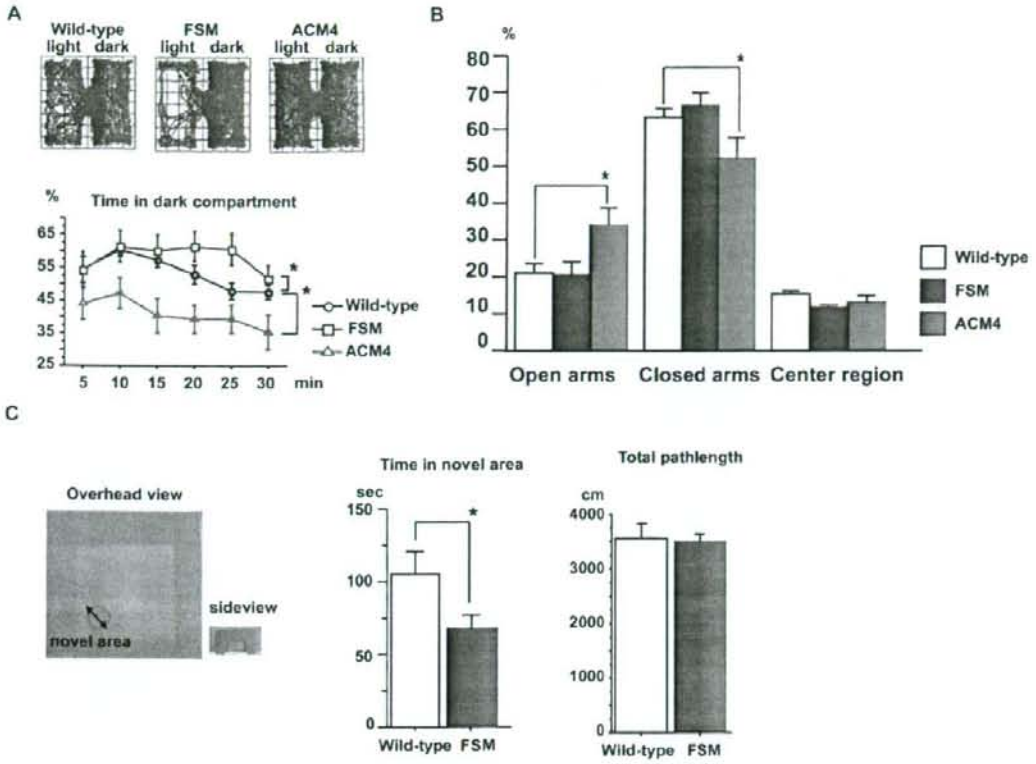

Figure 3. Activin protein levels in the brain modulate anxiety-related behavior. (A) Upper panels, typical traces in the light and dark test for each genotype. Lower panels, time (%) spent in the dark compartment was measured over 30 min. Wild-type littermates (black circles), n = 34; FSM (blue squares), n = 18; ACM4 (red triangles), n = 11. *, $p<0.05$, Fisher's test. (B) Statistical analyses of elevated plus-maze. Wild-type littermates, n = 26; FSM, n = 7; ACM4, n = 11. p values indicate ANOVA for genotype effect. *, $p<0.05$; t-test. (C) Left panels shows the apparatus used for the novel-area accessing test. Arrows indicate points of entry to the cylinder. Small picture shows side view of the cylinder. Bar graphs show time spent in novel area (inside cylinder) and distance traveled during 10 min testing. *, $p<0.05$, t-test. Results are shown as mean±s. e. m.
doi:10.1371/journal.pone.0001869.g003

injections (**Fig. 4E**) was monitored at various developmental stages. The number of BrdU- and NeuN-double positive cells was normal at the 1-week stage in FSM mice, suggesting a normal differentiation rate. However, a marked decrease was observed in the number of BrdU- and NeuN-double positive cells at 2- and 3-week stages compared with wild-type littermates. Therefore, in FSM mice, the survival of newly generated neurons is significantly decreased. This indicates that activin signal is essential for the maintenance of newly generated neurons. Activin overexpression did not enhance the number of BrdU- and NeuN-double positive cells at 4 weeks, suggesting that activin overexpression is not sufficient for enhancement of adult neurogenesis (**Fig. 4C**).

Taken together, FSM and ACM4 mice showed opposite phenotypes in behavior. Furthermore, decrease in neurogenesis in FSM mice was partially rescued in FSM/ACM4 double transgenic mice. These results strongly suggest that the observed effects of overexpression, either follistatin or activin, are not positional transgene effects such as insertional mutations.

Discussion

There is a marked overlap and coincidence between anxiety and depression [1–3]. Depression is a serious disorder in our current society. Many popularly prescribed antidepressant drugs work to modulate monoamine neurotransmission, and take six to eight weeks to exert their effects [3]. Each drug is efficacious in only 60–70% of patients. Therefore, a conceptually novel antidepressant that acts rapidly and safely in a high proportion of patients would be highly advantageous [3]. We show here that activin in the forebrain bi-directionally influences anxiety-related behavior. Depression is usually seen in anxiety patients, and anxiety is often reported in depressed patients [1–3]. A recent paper by Dow *et al.* showed that activin infusion into the hippocampus produced an antidepressant-like effect [36]. Therefore, the level of activin in the hippocampus modulates both depressive and anxiety-related behavior. Therefore, activin may represent a new contributing factor for the modulation of anxiety. The transgenic mice used in this study may be useful for screening compounds in the development of new mechanistically-novel anti-depressant drugs.

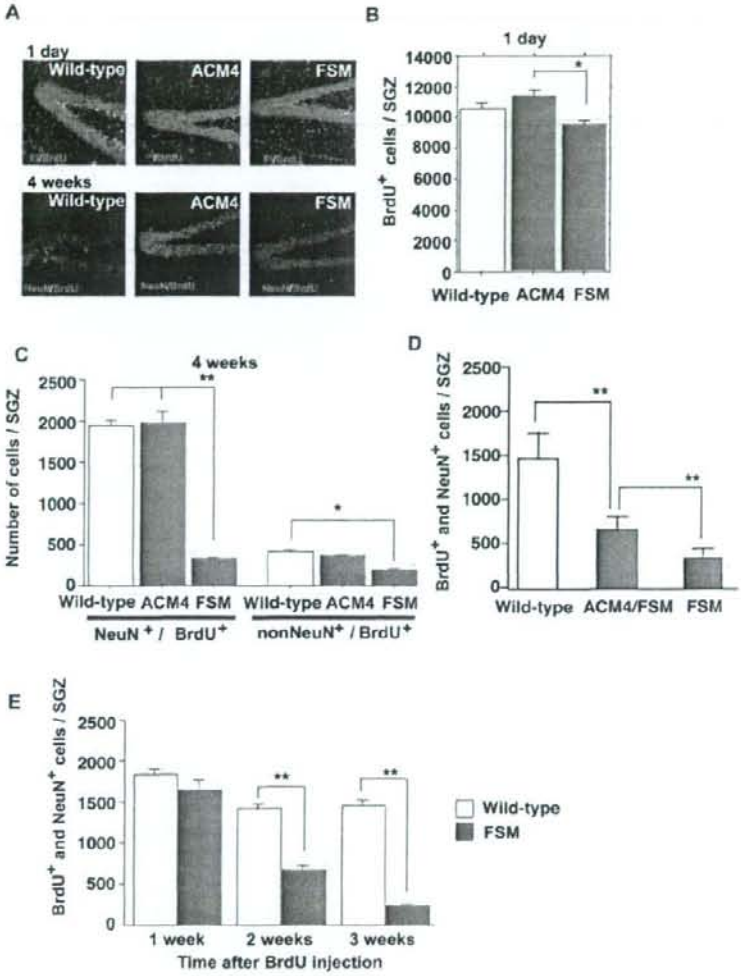

Figure 4. Activin signal is essential for survival of newly generated neurons. (A) BrdU positive cells (green) in the SGZ. Mice were sacrificed 1 day (upper panels) or 4 weeks (lower panels) after BrdU administration. At 4 weeks, most BrdU-positive cells were co-labeled with NeuN (red), a marker for mature neurons. Propidium iodide (PI, red) was used as a nuclear marker. (B) Number of BrdU-positive cells in the SGZ. The Y-axis indicates the number of BrdU-positive cells of the entire hippocampus. ACM4 had more BrdU-positive cells than FSM (wild-type, n = 21 animals; ACM4, n = 6 animals; FSM, n = 10 animals). (C) Number of BrdU-positive cells differentiated to neurons ($NeuN^+/BrdU^+$) or differentiated to another cell type ($non\text{-}NeuN^+/BrdU^+$) in the SGZ (wild-type, n = 25; ACM4, n = 14; FSM, n = 9). Animals were sacrificed 4 weeks after BrdU administration. (D) Number of BrdU- and NeuN-double positive cells in the SGZ (wild-type, n = 32; ACM4/FSM, n = 9; FSM, n = 14). Animals were sacrificed 4 weeks after BrdU administration. (E) Number of BrdU/NeuN-double positive cells in the SGZ. Animals were sacrificed 1, 2, or 3 weeks after BrdU administration. At the 2-week stage (wild-type, n = 7; FSM, n = 8), but not at the 1-week stage (wild-type, n = 7; FSM, n = 9), the number of double positive cells was significantly decreased in FSM mice compared with wild-type littermates. Error bars indicate the s. e. m. *, $p<0.05$; **, $p<0.01$; t-test.
doi:10.1371/journal.pone.0001869.g004

Materials and Methods

Transgene construction and generation of transgenic mice

Coding region for mouse activin or human follistatin was amplified by PCR using specific PCR primers designed to add a Kozac sequence at the N-terminus and a myc-tag sequence at the C-terminus. The resulting cDNAs were cloned into pcDNAI (Invitrogen) to append an SV40 intron/polyadenylation signal at the 3'-end. These constructs were inserted into the Not I site of pMM403 vector (kindly provided by Dr. M. Mayford) [18] which contains the alpha calcium/calmodulin-dependent protein kinase II (αCaMKII) promoter to generate pCaM-activin-Myc and pCaM-follistatin-Myc plasmids. *Sfi* I fragments were isolated from

pCaM-activin-Myc or pCaM-follistatin-Myc and microinjected into the pronuclei of one-cell embryos of C57BL/6J mice to produce transgenic mice [37]. Microinjected embryos were transferred to the oviducts of pseudo-pregnant females. Founder transgenic mice were identified by Southern blot analyses and PCR analysis with genomic DNA prepared from tail, and bred with C57BL/6J mice. Forward (f) and reverse (r) PCR primers for genotyping were as follows: ACM, f-5′-CACCCACTAGCCGT-TACCAT-3′and r-5′-ATCCTCTCAGCCAAAGCAAG-3′; FSM, f-5′-GAGGTAGGAAGAGCGATGAT-3′and r-5′-CTCCATCA-TTCCCACAGAGA -3′. C57BL/6J mice were purchased from Clea Japan Inc. (Tokyo, Japan)

ELISA analysis

After removal of the brain, each neuronal tissue (hippocampus, cortex, cerebellum and medulla) was quickly dissected out. Tissues were homogenized in lysis buffer [5 mM Tris-HCl, pH 8.0, 0.32 M sucrose, protease inhibitor cocktail (Sigma)], and homogenates were centrifuged at 20,000×g at 4°C for 10 min. Supernatant was collected and assayed for quantification of total protein with the BCA™ Protein Assay Kit (Pierce). Follistatin and activin levels were assayed by using commercial ELISA kits (Human Follistatin Immunoassay, AN'ALYZA and Activin-A ASSAY, Oxford Bio-Innovation, respectively).

Neurogenesis

Male mice at 5 weeks-old received daily intraperitoneal injections of BrdU (Sigma) in 0.9% NaCl solution (75mg/kg, three times per day for three days). Animals were sacrificed with an overdose of anesthetics and perfused transcardially with 0.9% saline followed by 4% paraformaldehyde (PFA) in PBS. Brains were stored in fixative (4% PFA in PBS) for 3 h at 4°C, and incubated overnight in 30% sucrose, and then immersed in dry ice powder. A cryostat was used to collect sagittal sections of 14-μm thickness. The sections were boiled for 10 min, and then treated with 2M HCl for 30 min. After rinsing in 0.1 M boric acid (pH 8.5) for 10 min, tissues were incubated in 1% H_2O_2 in PBS for 30 min, and then blocked with 0.1% BSA and 3% goat serum in PBS containing with 0.1% Tween20 (PBST) at room temperature for 1 h. After blocking, tissues were incubated with blocking solution containing rat monoclonal anti-BrdU (1:250; Accurate) and mouse monoclonal anti-NeuN (1:200; Chemicon) antibodies. Sections were then incubated with anti-rat IgG-FITC and anti-mouse IgG-Rhodamine.

For quantification, three consecutive serial sections at section-interval 13 were used for counting BrdU-positive cells though an ×40 objective (BX41, OLYMPUS) in a genotype-blinded manner. Total number of BrdU-positive cells was obtained by multiplying the number of BrdU-positive cells counted in all the sections by 13/3. Figures were imaged by confocal microscopy operated under manual control (LSM5 PASCAL, ZEISS).

Animal care and data analysis

All procedures involving mice were performed in compliance with National Institutes of Health guidelines and were approved by the Animal Care and Use Committee of Mitsubishi Kagaku Institute of Life Sciences, MITILS. We abided by MITILS guidelines on animal husbandry. All behavior experiments were conducted in a blinded fashion on male, heterozygous transgenic mice and their wild-type littermates (5–6 months). Two weeks before behavioral analysis, animals were housed individually in plastic cages and maintained on a 12:12-h light:dark cycle. Food and water were provided *ad libitum*. For five days before behavioral analysis, the mice were handled daily. Statistical analyses were conducted using StatView (Abacus Concepts). Values were expressed as mean±s. e. m..

In situ hybridization

To detect transgene expression the SV40 poly A signal sequence, which is found in each transgene, was used as an antisense probe (Fig 1A). To prepare the probe, this region was subcloned into pBluescript II (Stratagene) to generate pSV40. pSV40 was digested with BamHI to generate DNA template for *in vitro* transcription of antisense cRNA probe. Digoxigenin-labeled antisense cRNA probe was produced by transcription with T7 polymerase. For hybridization experiments, animals were sacrificed with an overdose of anesthetics, and the brain was dissected and immediately frozen on dry ice. Cryostat sections (20-μm thickness) were cut and mounted onto polylysine-coated glass slides. Sections were air-dried and stored at −80°C until use in hybridization. *In situ* hybridization was carried out as described previously [38].

Behavioral analysis

Behavioral experiments were basically carried out as described previously [39]. In the open field test, spontaneous locomotor activity was measured in a square arena (50×50×30 cm; Muromachi Kikai, Japan) by using a device outfitted with photo-beam detectors for monitoring horizontal and vertical activity, namely, distance traveled, time spent in locomotion, rearing counts and time in rearing. For statistical analysis on the percentage pathlength in the center region, we used ImageJ program (developed at the U. S. National Institutes of Health, and available on the Internet at http://rsb.info.nih.gov/ij/), Mice were allowed to explore freely while data was collected for 30 min. In the light and dark test, the square arena was divided into light and dark compartments. Data was collected as mice were allowed to freely traverse the arena among the two compartments for 30 min.

The elevated plus-maze comprises areas of two opposing open arms (25×5×0.5 cm) and two opposing enclosed arms (25×5×15 cm), connected by a central platform (O'HARA & Co, Japan). Mice were placed in the center area, and allowed to explore for 10 min. Their activity was recorded by video camera. Results were analyzed on a Macintosh computer using Image EP2.13 (O'HARA & Co), modified software of the public domain NIH Image program (developed at the U. S. National Institutes of Health, and available on the Internet at http://rsb.info.nih.gov/nih-image/).

In the novel-area accessing test (**Fig. 3C**), mice were placed in the center of a box (60×60×50 cm) for 10 min on the first day in order to habituate the apparatus. The next day mice were placed in the same box to which a novel cylinder (13 cm in diameter) with two entrances (6×3.5 cm) was added. Mice were allowed to explore for 10 min, while their activity was recorded by video camera. Results were analyzed on a Macintosh computer using Image OEC 1.02r1 (O'HARA & Co), a modified software of the public domain NIH Image program.

Supporting Information

Figure S1 Traction test indicates that grip strength was comparable between transgenic mice and wild-type littermates. Forelimb grip strength was quantitatively assessed using a spring strain gauge (O'HARA & Co., Japan). Animals held by the tail grasped a wire netting and were gently pulled away from the bar with a smooth steady pull until they released the wire netting. The Y-axis indicates grip strength (g).

Found at: doi:10.1371/journal.pone.0001869.s001 (0.16 MB TIF)

Figure S2 Transgene expression was not detected in the internal organs of FSM and ACM4 mice. RT-PCR-based identification of transgene expression was carried out in various internal organs. Transgene plasmid DNA and total cellular RNA prepared from cortex of each transgenic mice line served as a positive control. Water and total cellular RNA from cortex of wild-type mice served as a negative control. Actin gene was used as an internal control. Unspliced products were detected at the upper position of mature and spliced product when transgene plasmid DNA or ACM4's cortex RNA were used as a template. To rule out the possibility that genomic DNA was amplified, we performed RT-PCR without reverse transcription (middle row panels, RT-), which showed no signals.
Found at: doi:10.1371/journal.pone.0001869.s002 (0.56 MB TIF)

Figure S3 Nissl staining of the coronal brain section from wild-type, FSM and ACM4. Lower panels, high magnification images of the hippocampus. Scale bar, 500 μm. Method. Animals were sacrificed with an overdose of anesthetics, and the brain was dissected and immediately frozen on dry ice. Cryostat sections (18-μm thickness) were cut and mounted onto polylysine-coated glass slides. Sections were air-dried and stored at −80°C until use. Slides were immersed in the 10% formalin solution for 30 min at 4°C for the fixation, and washed twice with PBS for 15 min at room temperature. Slides were then stained with 0.1% Cresyl Violet for 10 min. They were differentiated in H_2O for 3–5 min and then dehydrated through 70%, 95%, 100% and 100% alcohol. They were then put in xylene and cover-slipped.
Found at: doi:10.1371/journal.pone.0001869.s003 (0.76 MB TIF)

Figure S4 Analysis of forced swimming test [wild-type littermates (black circles), n = 18; FSM (blue squares), n = 8] on day 2. The immobilizing time (sec) was plotted for each minute. No significant genotype effect was observed for FSM. On day 1, mice were placed in a container with water at a depth of 20 cm (23–25°C) for 15 min. and forced to swim as they were unable to touch the bottom with their hind limbs. On day 2, the mice were placed back into 20 cm deep water for 5 min. When mice were unable to avoid the forced swimming, they exhibited immobility. Immobility was monitored by infra-red detector (CompACT FSS, Muromachi Kikai).
Found at: doi:10.1371/journal.pone.0001869.s004 (0.13 MB TIF)

Acknowledgments

We thank Drs. S. Ikegami and Y. Saitoh for valuable suggestions on behavior tests; Dr. M. Mayford for providing the plasmid containing αCaMKII promoter; Dr. M. Matsushita for critical reading of the manuscript; E. Tokunaga for genotyping the transgenic mice; Dr. S. Kamijo, Ms. M. Matsuo, Ms. K. Kawaguchi, Ms. C. Sutou and Mr. S. Tayama for breeding and maintaining the transgenic mice; and members of the Inokuchi laboratory for helpful discussions. We thank two anonymous reviewers for constructive criticism and superb suggestions for experiments to strengthen the study.

Author Contributions

Conceived and designed the experiments: KI HA. Performed the experiments: HA AM RM MY. Analyzed the data: HA. Contributed reagents/materials/analysis tools: SK KT. Wrote the paper: KI HA. Other: Supervised the entire project: KI.

References

1. Gryan JF, Holmes A (2005) The ascent of mouse: advances in modelling human depression and anxiety. Nat Rev Drug Discov 4: 775–790.
2. Kalueff AV, Wheaton M, Murphy DL (2007) What's wrong with my mouse model? Advances and strategies in animal modeling of anxiety and depression. Behav Brain Res 179: 1–18.
3. Wong ML, Licinio J (2004) From monoamines to genomic targets: a paradigm shift for drug discovery in depression. Nat Rev Drug Discov 3: 136–151.
4. Dranovsky A, Hen R (2006) Hippocampal neurogenesis: regulation by stress and antidepressants. Biol Psychiatry 59: 1136–1143.
5. Earnheart JC, Schweizer C, Crestani F, Iwasato T, Itohara S, et al. (2007) GABAergic control of adult hippocampal neurogenesis in relation to behavior indicative of trait anxiety and depression states. J Neurosci 27: 3845–3854.
6. Bilezikjian LM, Blount AL, Donaldson CJ, Vale WW (2006) Pituitary actions of ligands of the TGF-beta family: activins and inhibins. Reproduction 132: 207–215.
7. Cameron VA, Nishimura E, Mathews LS, Lewis KA, Sawchenko PE, et al. (1994) Hybridization histochemical localization of activin receptor subtypes in rat brain, pituitary, ovary, and testis. Endocrinology 134: 799–808.
8. Funaba M, Murata T, Fujimura H, Murata E, Abe M, et al. (1997) Immunolocalization of type I or type II activin receptors in the rat brain. J Neuroendocrinol 9: 105–111.
9. Shoji H, Tsuchida K, Kishi H, Yamakawa N, Matsuzaki T, et al. (2000) Identification and characterization of a PDZ protein that interacts with activin type II receptors. J Biol Chem 275: 5485–5492.
10. Hirao K, Hata Y, Ide N, Takeuchi M, Irie M, et al. (1998) A novel multiple PDZ domain-containing molecule interacting with N-methyl-D-aspartate receptors and neuronal cell adhesion proteins. J Biol Chem 273: 21105–21110.
11. Tretter YP, Hertel M, Munz B, ten Bruggencate G, Werner S, et al. (2000) Induction of activin A is essential for the neuroprotective action of basic fibroblast growth factor in vivo. Nat Med 6: 812–815.
12. Andreasson K, Worley PF (1995) Induction of beta-A activin expression by synaptic activity and during neocortical development. Neuroscience 69: 781–796.
13. Inokuchi K, Kato A, Hiraia K, Hishimuna F, Inoue M, et al. (1996) Increase in activin beta A mRNA in rat hippocampus during long-term potentiation. FEBS Lett 382: 48–52.
14. Fukazawa Y, Saitoh Y, Ozawa F, Ohta Y, Mizuno K, et al. (2003) Hippocampal LTP is accompanied by enhanced F-actin content within the dendritic spine that is essential for late LTP maintenance in vivo. Neuron 38: 447–460.
15. Shoji-Kasai Y, Ageta H, Hasegawa Y, Tsuchida K, Sugino H, et al. (2007) Activin increases the number of synaptic contacts and the length of dendritic spine necks by modulating spinal actin dynamics. J Cell Sci 120: 3830–3837.
16. Matzuk MM, Kumar TR, Bradley A (1995) Different phenotypes for mice deficient in either activins or activin receptor type II. Nature 374: 356–360.
17. Matzuk MM, Kumar TR, Vassalli A, Bickenbach JR, Roop DR, et al. (1995) Functional analysis of activins during mammalian development. Nature 374: 354–356.
18. Mayford M, Bach ME, Huang YY, Wang L, Hawkins RD, et al. (1996) Control of memory formation through regulated expression of a CaMKII transgene. Science 274: 1678–1683.
19. Kida S, Josselyn SA, de Ortiz SP, Kogan JH, Chevere I, et al. (2002) CREB required for the stability of new and reactivated fear memories. Nat Neurosci 5: 348–355.
20. Brinster RL, Chen HY, Trumbauer ME, Yagle MK, Palmiter RD (1985) Factors affecting the efficiency of introducing foreign DNA into mice by microinjecting eggs. Proc Natl Acad Sci U S A 82: 4438–4442.
21. Munz B, Smola H, Engelhardt F, Bleuel K, Brauchle M, et al. (1999) Overexpression of activin A in the skin of transgenic mice reveals new activities of activin in epidermal morphogenesis, dermal fibrosis and wound repair. Embo J 18: 5205–5215.
22. Wankell M, Munz B, Hubner G, Hans W, Wolf E, et al. (2001) Impaired wound healing in transgenic mice overexpressing the activin antagonist follistatin in the epidermis. Embo J 20: 5361–5372.
23. Guo Q, Kumar TR, Woodruff T, Hadsell LA, DeMayo FJ, et al. (1998) Overexpression of mouse follistatin causes reproductive defects in transgenic mice. Mol Endocrinol 12: 96–106.
24. Sugino H, Sugino K, Hashimoto O, Shoji H, Nakamura T (1997) Follistatin and its role as an activin-binding protein. J Med Invest 44: 1–14.
25. Spear LP (2000) The adolescent brain and age-related behavioral manifestations. Neurosci Biobehav Rev 24: 417–463.
26. Stansfield KH, Kirstein CL (2007) Chronic cocaine or ethanol exposure during adolescence alters novelty-related behaviors in adulthood. Pharmacol Biochem Behav 86: 637–642.
27. Tang YP, Shimizu E, Dube GR, Rampon C, Kerchner GA, et al. (1999) Genetic enhancement of learning and memory in mice. Nature 401: 63–69.
28. Gage FH (2002) Neurogenesis in the adult brain. J Neurosci 22: 612–613.
29. Nakatomi H, Kuriu T, Okabe S, Yamamoto S, Hatano O, et al. (2002) Regeneration of hippocampal pyramidal neurons after ischemic brain injury by recruitment of endogenous neural progenitors. Cell 110: 429–441.
30. Kokaia Z, Lindvall O (2003) Neurogenesis after ischaemic brain insults. Curr Opin Neurobiol 13: 127–132.
31. Shors TJ, Miesegaes G, Beylin A, Zhao M, Rydel T, et al. (2001) Neurogenesis in the adult is involved in the formation of trace memories. Nature 410: 372–376.

32. Kempermann G, Gage FH (2002) Genetic determinants of adult hippocampal neurogenesis correlate with acquisition, but not probe trial performance, in the water maze task. Eur J Neurosci 16: 129–136.
33. Mirescu C, Peters JD, Gould E (2004) Early life experience alters response of adult neurogenesis to stress. Nat Neurosci 7: 841–846.
34. Nakagawa S, Kim JE, Lee R, Malberg JE, Chen J, et al. (2002) Regulation of neurogenesis in adult mouse hippocampus by cAMP and the cAMP response element-binding protein. J Neurosci 22: 3673–3682.
35. Santarelli L, Saxe M, Gross C, Surget A, Battaglia F, et al. (2003) Requirement of hippocampal neurogenesis for the behavioral effects of antidepressants. Science 301: 805–809.
36. Dow AL, Russell DS, Duman RS (2005) Regulation of activin mRNA and Smad2 phosphorylation by antidepressant treatment in the rat brain: effects in behavioral models. J Neurosci 25: 4908–4916.
37. Hogan B, Beddington R, Costantini F, Lacy E (1994) Manipulating the Mouse Embryo: A LABORATORY MANUAL. Cold Spring Harbor, New York: Cold Spring Harbor Laboratory Press.
38. Matsuo R, Asada A, Fujitani K, Inokuchi K (2001) LIRF, a gene induced during hippocampal long-term potentiation as an immediate-early gene, encodes a novel RING finger protein. Biochem Biophys Res Commun 289: 479–484.
39. Ikegami S, Inokuchi K (2000) Antisense DNA against calcineurin facilitates memory in contextual fear conditioning by lowering the threshold for hippocampal long-term potentiation induction. Neuroscience 98: 637–646.

Transduction Efficiency and Immune Response Associated With the Administration of AAV8 Vector Into Dog Skeletal Muscle

Sachiko Ohshima[1,2], Jin-Hong Shin[1,3], Katsutoshi Yuasa[1,4], Akiyo Nishiyama[1], Junichi Kira[2], Takashi Okada[1] and Shin'ichi Takeda[1]

[1]Department of Molecular Therapy, National Institute of Neuroscience, National Center of Neurology and Psychiatry, Tokyo, Japan; [2]Department of Neurology, Neurological Institute, Graduate School of Medical Sciences, Kyushu University, Fukuoka, Japan; [3]Department of Neurology, Graduate School of Medicine, Pusan National University, Busan, Republic of Korea; [4]Research Institute of Pharmaceutical Sciences, Faculty of Pharmacy, Musashino University, Tokyo, Japan

Recombinant adeno-associated virus (rAAV)-mediated gene transfer is an attractive approach to the treatment of Duchenne muscular dystrophy (DMD). We investigated the muscle transduction profiles and immune responses associated with the administration of rAAV2 and rAAV8 in normal and canine X-linked muscular dystrophy in Japan ($CXMD_J$) dogs. rAAV2 or rAAV8 encoding the *lacZ* gene was injected into the skeletal muscles of normal dogs. Two weeks after the injection, we detected a larger number of β-galactosidase-positive fibers in rAAV8-transduced canine skeletal muscle than in rAAV2-transduced muscle. Although immunohistochemical analysis using anti-CD4 and anti-CD8 antibodies revealed less T-cell response to rAAV8 than to rAAV2, β-galactosidase expression in rAAV8-injected muscle lasted for <4 weeks with intramuscular transduction. Canine bone marrow-derived dendritic cells (DCs) were activated by both rAAV2 and rAAV8, implying that innate immunity might be involved in both cases. Intravenous administration of rAAV8-*lacZ* into the hind limb in normal dogs and rAAV8-*microdystrophin* into the hind limb in $CXMD_J$ dogs resulted in improved transgene expression in the skeletal muscles lasting over a period of 8 weeks, but with a declining trend. The limb perfusion transduction protocol with adequate immune modulation would further enhance the rAAV8-mediated transduction strategy and lead to therapeutic benefits in DMD gene therapy.

Received 16 March 2008; accepted 17 September 2008; published online 21 October 2008. doi:10.1038/mt.2008.225

INTRODUCTION

Duchenne muscular dystrophy (DMD) is an inherited disorder causing progressive deterioration of skeletal and cardiac muscles because of mutations in the dystrophin gene. No effective treatment has been established despite the development of various novel therapeutic strategies including pharmacologic and gene therapies. Dystrophin-deficient *mdx* mice and dystrophin-utrophin double-knockout mice are the animal models most widely used to evaluate therapeutic efficacy, although the symptoms of *mdx* mice are not comparable to those of human DMD patients. Dystrophin-deficient canine X-linked muscular dystrophy was found in a golden retriever,[1,2] and we have established a Beagle-based model of canine X-linked muscular dystrophy in Japan ($CXMD_J$) dogs.[3] The clinical and pathological characteristics of the dystrophic dogs are more similar to those of DMD patients than murine models.[3]

The recombinant adeno-associated virus (rAAV) can be used for delivering genes to muscle fibers. Several serotypes of rAAV exhibit a tropism for striated muscles.[4,5] Intramuscular or intravenous administration of rAAV carrying the microdystrophin gene was reported to restore specific muscle force and extend the lifespan in dystrophic mice.[6,7] In contrast to the success of transgene delivery in mice, rAAV2 or rAAV6 delivery to canine striated muscles without immunosuppression resulted in insufficient transgene expression, and rAAV evoked strong immune responses.[8,9] An assay of interferon-γ released from murine and canine splenocytes suggested that the immune responses against rAAV and transgene products in mice and in dogs are dissimilar.[8] Uptake of rAAV2 by human dendritic cells (DCs) and T-cell activation in response to the AAV2 capsid have been reported,[10] indicating that DCs play key roles in the immune response against rAAV-mediated transduction. On the other hand, other serotypes, including rAAV8, that are capable of whole-body skeletal muscle expression after intravenous administration,[4,5]induce less T-cell activation.[11] We hypothesized that the level of activation of canine DCs by rAAV8 might be lower than that achieved by rAAV2. However, the transduction profile and immune response in the rAAV8-injected dog skeletal muscle have not been elucidated.

In this study, we chose to use intramuscular injections under ultrasonographic guidance so as to minimize the inflammatory reaction caused by incisional intramuscular injection.[8] In

Correspondence: *Shin'ichi Takeda or Takashi Okada, Department of Molecular Therapy, National Institute of Neuroscience, National Center of Neurology and Psychiatry, 4-1-1 Ogawa-higashi, Kodaira, Tokyo 187-8502, Japan. E-mail: takeda@ncnp.go.jp or t-okada@ncnp.go.jp*

addition, intravascular delivery was performed as a form of limb perfusion, in an attempt to bypass the immune activation of DCs in the injected muscle.[12] We investigated the transgene expression and host immune response to two distinct serotypes of rAAV in normal and dystrophic dogs after direct intramuscular injection and after limb perfusion.

RESULTS

Extensive expression of β-galactosidase in rAAV8-transduced muscles in wild-type dogs

We administered nonincisional intramuscular injections under ultrasonographic guidance so as to minimize injury. With incisional injection, the ordinary method of intramuscular viral administration in dogs,[8] the skin is opened to identify the individual muscles. This may enhance the immune reaction by recruiting inflammatory cells for wound healing. After nonincisional injection of rAAV2-*lacZ*, faint β-galactosidase (β-gal) expression was detected, whereas lymphocyte infiltration still occurred (**Supplementary Figure S1**). To investigate the transduction efficiency of rAAV8 in canine skeletal muscle, normal dogs were transduced with rAAV-*lacZ* serotypes 2 and 8 (**Table 1**). Prominent expression of β-gal was observed in the rAAV8-*lacZ*-injected muscles, whereas the rAAV2-*lacZ*-injected muscles showed minimal transgene expression (**Figure 1**). While β-gal expression in the rAAV8-injected muscle was correlated with the viral dose, β-gal expression in the rAAV2-injected muscle was not augmented with viral dose escalation. However, rAAV8-*lacZ*-injected muscles, which showed extensive β-gal expression at 2 weeks, also exhibited reduced expression at 4 weeks after the injection, thereby suggesting that the transgene product had immunogenicity (**Supplementary Figure S2**).

To evaluate the difference in transduction efficiency between rAAV2 and rAAV8 at 2 weeks after the injection, relative quantifications of the vector genome and mRNA were performed. The result demonstrated higher transduction rates in the rAAV8-injected muscles as increasing amounts of the vector were administered (**Figure 2a,b**). The amount of protein expression was also well correlated with that of transgenic DNA (**Figure 2c**, **Supplementary Table S1**). Immunohistochemical analysis revealed that the rAAV2-injected muscles showed much more infiltration of $CD4^+$ and $CD8^+$ T lymphocytes in the endomysial space than the rAAV8-injected muscles did (**Figure 3a**). mRNA levels of TGF-β1 and IL-6 (representative markers of inflammation) in the rAAV-injected muscles were standardized with the β-gal expression. rAAV2-injected muscles had higher TGF-β1 and IL-6 expression than rAAV8-transduced muscles (**Supplementary Figure S3**). We also examined humoral immune responses against the rAAV particles in the sera of rAAV-injected dogs. The levels of serum IgG in reaction to rAAV2 or rAAV8 gradually increased with time in both serotypes (**Figure 3b**). These results suggest

Table 1 Summary of gene transduction experiments

									Transgene expression[d]			Cellular infiltration[e]		
Dog ID	Sex	Age[a]	BW[b]	rAAV serotype	Transgene	Route	Muscle	Vector dose[c]	2 weeks	4 weeks	8 weeks	2 weeks	4 weeks	8 weeks
2201MN	M	10	4.5	2	lacZ	i.m.	TA, ECR	1×10^{11}	−	−		−	++	
3004MN	M	5	2.8	2	lacZ	i.m.	TA, ECR	1×10^{11}	±	−		+	±	
3007FN	F	5	2.5	2	lacZ	i.m.	TA, ECR	1×10^{11}	±	±		++	++	
2204FN	F	10	2.5	2	lacZ	i.m.	TA, ECR	1×10^{12}	−	−		+	++	
2801FN	F	10	5.2	2	lacZ	i.m.	TA, ECR	1×10^{12}	+	−		+	++	
2901MN	M	6	2.8	2	lacZ	i.m.	TA, ECR	1×10^{12}	−			±		
7M48	M	7	3.3	2	lacZ	i.m.	TA, ECR	1×10^{12}	−			+		
2206FN	F	10	3.0	2	lacZ	i.m.	TA, ECR	1×10^{13}	±	±		+	++	
2205MN	M	10	4.2	8	lacZ	i.m.	TA, ECR	1×10^{11}	++	±		−	++	
2905MN	M	6	2.8	8	lacZ	i.m.	TA, ECR	1×10^{11}	±			−		
NL52F	F	10	3.5	8	lacZ	i.m.	TA, ECR	1×10^{12}	+++			±		
2106FN	F	6	3.2	8	lacZ	i.m.	TA, ECR	1×10^{12}	+++	−		−	++	
7M49	F	6	3.2	8	lacZ	i.m.	TA, ECR	1×10^{12}		±	−		++	±
2109FMN	M	7	3.3	8	lacZ	i.m.	TA, ECR	1×10^{12}	+++			−		
2903MN	M	6	3.2	8	lacZ	i.m.	TA, ECR	1×10^{12}	+++			±		
2209MN	M	10	4.3	8	lacZ	i.m.	TA, ECR	1×10^{13}	+++	±		±	+++	
2309FA	F	6	3.2	8	M3	i.m.	TA, ECR	1×10^{12}	±	+				
LH49F	F	8	3.3	8	lacZ	i.v.		1×10^{14}	+++			+		
3805MN	M	6	3.5	8	lacZ	i.v.		1×10^{14}		+++	+		+	+
2704FA	F	8	3.6	8	M3	i.v.		1×10^{14}	+	+++				
4001MA	M	6	3.2	8	M3	i.v.		1×10^{14}		+++	+			

BW, body weight; F, female; M, male.

[a]Age at injection (weeks). [b]BW at injection (kg). [c]Vectors (vg/ml) were intramuscularly (i.m.) injected into extensor carpi radiolis (ECR) (1 ml) and tibialis anterior (TA) (2 ml) on both sides. Vectors were also intravenously (i.v.) injected into the lateral saphenous vein (vg/kg/limb) by using limb perfusion method. [d]β-Gal or microdystrophin-positive fibers per 3,000 fibers: −, 0; ±, <100; +, <300; ++, <1,000; +++, >1,000. [e]Infiltrating cells: −, not detected; ±, a few; +, moderate; ++, extensive.

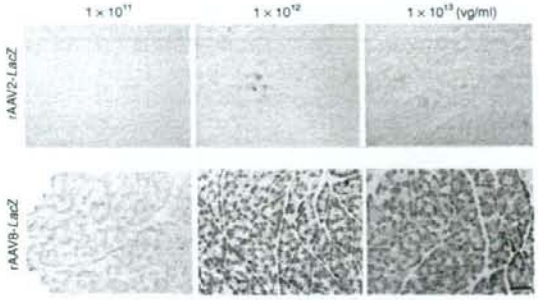

Figure 1 Canine skeletal muscles stained for β-galactosidase. Two milliliters of rAAV2-*lacZ* or rAAV8-*lacZ* (1×10^{11}–10^{13} vg/ml) were injected intramuscularly into the tibialis anterior (TA) muscle of normal dogs ($n = 16$) under ultrasonographic guidance. The muscles were biopsied 2 weeks after the injection. Upper: rAAV2-*lacZ*-injected TA muscles, Lower: rAAV8-*lacZ*-injected TA muscles. Bar = 200 μm.

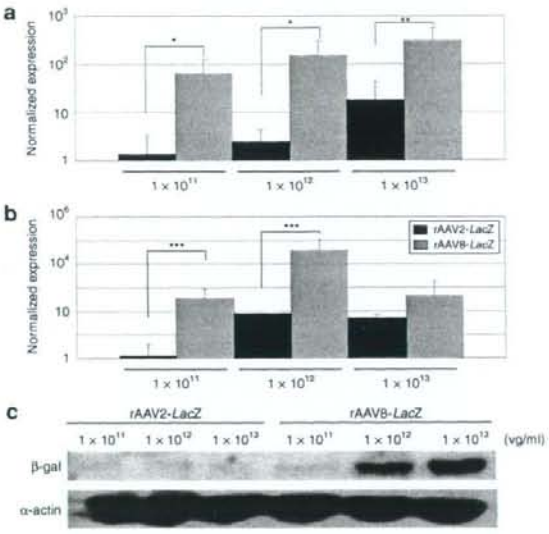

Figure 2 Quantification of viral vector genome, mRNA, and transgene expression. (a) Relative quantification of genomic PCR for rAAV2-*lacZ*-injected muscle (black bars) or rAAV8-*lacZ*-injected muscle (gray bars). DNA samples were extracted from the TA muscles. $^{*}P < 0.05$. $^{**}P < 0.01$. Error bars represent 2 SD. **(b)** Relative quantification showed more extensive β-gal mRNA expression caused by rAAV8-*lacZ* (gray bars) as compared to that caused by rAAV2-*lacZ* (black bars). 18S rRNA was used for an internal control. $^{***}P < 0.05$. Error bars represent 2 SD. **(c)** Western blots of β-gal protein (120 kDa) and α-actin (42 kDa); the β-gal signal was normalized to α-actin for comparison.

that cellular and humoral immune responses are elicited in both rAAV2- and rAAV8-transduced muscles.

Bone marrow-derived DC reactions to rAAV2 and rAAV8

We next cultured bone marrow-derived DCs to investigate their response to rAAV injection in dogs. Flow cytometric analyses of these cells at 7 days of culture revealed marked expressions of CD11c and MHC class II molecules on the surface (**Figure 4a,b**). The DCs were cultured with the rAAV-*luciferase* of either serotype 2 or 8 for 48 hours to evaluate transduction efficiency, or cultured with rAAV-*lacZ* for 4 hours to investigate kinetic changes in mRNA. The luciferase assay showed that the transduction efficiency of rAAV2-*luciferase* in DCs was approximately two times that of rAAV8-*luciferase* (**Figure 4c**). mRNA levels of MyD88 and costimulating factors, such as CD80, CD86, and type I interferon (interferon-β, IFN-β) were elevated in both conditions (**Figure 4d**), suggesting that rAAV8 also induces a considerable degree of innate immune response in dog skeletal muscles. Although rAAV2-transduced DCs showed higher IFN-β expression than rAAV8-transduced DCs, the differences between the effects of rAAV2 and rAAV8 on the mRNA levels of MyD88, CD80, CD86, and IFN-β were not statistically significant.

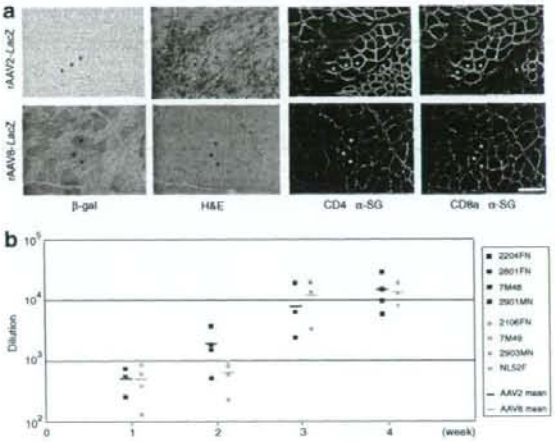

Figure 3 Immune response to rAAV. (a) Lymphocyte infiltration after rAAV transduction. Muscles were biopsied 2 weeks after rAAV2- or rAAV8-*lacZ* injection (2×10^{12} vg/muscle). Serial cross-sections were stained with β-gal and H&E, and were immunohistochemically stained with antibodies against canine CD4, CD8a (Alexa 568, red), and α-sarcoglycan (α-SG, Alexa 488, green). Upper: rAAV2-*lacZ*-injected TA muscle; lower: rAAV8-*lacZ*-injected TA muscle. Bar = 100 μm. **(b)** Humoral immune responses to rAAV capsid in dogs. Serum was collected weekly from rAAV2- or rAAV8-*lacZ*-injected dogs and analyzed for the presence of IgG antibody against the rAAV2 or rAAV8 capsid. The data represent dilution rates with 50% reactivity of anti-rAAV2 (black boxes) and anti-rAAV8 (gray boxes) capsid antibodies. The mean reconstitution values are shown as straight lines. Each symbol represents an individual dog that was injected with rAAV at 2×10^{12} vg/muscle.

Successful *microdystrophin* gene transfer with rAAV8 into dystrophic dogs

Dystrophin expression in normal skeletal muscle is localized on the sarcolemma, whereas it is totally absent in $CXMD_J$ dogs (**Supplementary Figure S4a,b**). Microdystrophin expression in the rAAV8-injected skeletal muscle of $CXMD_J$ dogs was maintained, even in the absence of any immunosuppressive therapy, for at least 4 weeks after the injection (**Table 1**). Previously, we had shown that microdystrophin expression of ca 20% was sufficient to achieve functional recovery in mdx mice[6]. However, the amount of the expression in intramuscularly injected muscles

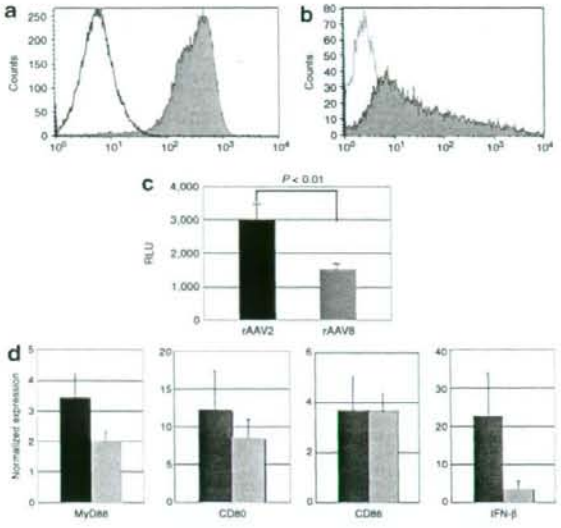

Figure 4 Responses of dendritic cells (DCs) to rAAV in dogs. Bone marrow-derived DCs were obtained from the humerus bones of dogs and cultured in RPMI (10% FCS, p/s) for 7 days with canine GM-CSF and IL-4. (**a**) Flow cytometric analysis of cell surface molecules on day 7. The cells were stained with PE-conjugated CD11c antibody and isotype control. (**b**) DCs were stained with FITC-conjugated MHC Class II antibody and isotype control. (**c**) DCs were transduced with rAAV-*luciferase* (1×10^4 vg/cell) for 48 hours. To analyze luciferase expression relating to the use of rAAV2 or rAAV8, relative light unit (RLU) ratios were measured. $^*P < 0.01$. Error bars represent s.e.m., $n = 8$. (**d**) DCs were transduced with 1×10^4 vg/cell of rAAV2 (black bars) or rAAV8-*lacZ* (gray bars) for 4 hours, and mRNA levels of MyD88, CD80, CD86, and IFN-β were analyzed. Untransduced cells were used as a control to demonstrate the relative value of expression. The results are representative of two independent experiments. Error bars represent s.e.m., $n = 3$.

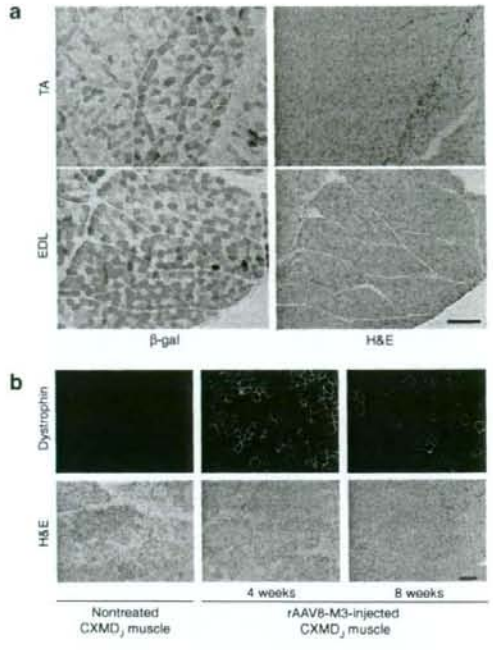

Figure 5 rAAV8-mediated muscle transduction using the limb perfusion method. (**a**) Transduction of normal dog with rAAV8-*lacZ*, using the limb perfusion method. Muscles were biopsied 2 weeks after the injection and stained with β-gal and H&E. TA, tibialis anterior, EDL, extensor digitorum longus. Bar = 200 μm. (**b**) Transduction of canine X-linked muscular dystrophy in Japan (CXMD$_J$) dog with rAAV8-*M3*. Muscles of CXMD$_J$ dogs were biopsied 4 and 8 weeks after limb perfusion with rAAV8-*M3*. Samples were immunohistochemically stained with anti-dystrophin antibody (dys2, NCL). Left: nontreated CXMD$_J$ muscle. Middle and right: muscles injected with rAAV-*M3* using limb perfusion method, examined at 4 or 8 weeks after the transduction. Bar = 100 μm.

seemed to be insufficient to produce the expected functional recovery (**Supplementary Figure S4c**).

For more efficient gene delivery by rAAV8, we tried a limb perfusion method in the hind limb through the lateral saphenous vein, in an attempt to prevent muscle damage due to direct injection and to bypass immune activation through DCs in the injected muscle. We had observed highly efficient β-gal expression in nearly all the muscles of the distal hind limb at 2 weeks after a single injection (**Table 1**, **Figure 5a**). We then injected rAAV8-*M3* into the hind limbs of CXMD$_J$ dogs, using the same method (**Table 1**). The induction of microdystrophin expression in the muscle at 4 weeks after intravascular injection was more efficient and free of noticeable immune response as compared to intramuscularly injected muscle (**Figure 5b**, **Supplementary Figure S4d**). These results suggest that the intravascular method is superior to the intramuscular method of administration. Although microdystrophin expression persisted at 8 weeks after injection of rAAV8-*M3*, the number of microdystrophin-positive cells at this time point was lower than in the muscles that were sampled at 4 weeks after injection. It is clear, therefore, that long-term microdystrophin expression can be obtained by the limb perfusion method, but that the expression does not last at the same level over a period of weeks. The same phenomenon was observed in rAAV8-*lacZ*-transduced muscles (**Supplementary Figure S5**).

DISCUSSION

In this article, we present evidence that the transfer of rAAV8-*lacZ* to canine skeletal muscles produces higher transgene expression with less lymphocyte proliferation than rAAV2-*lacZ* does, at 2 weeks after injection. Given the advantages of rAAV8, the administration of rAAV8-*M3* by limb perfusion produced extensive transgene expression in the distal limb muscles of CXMD$_J$ dogs without obvious immune responses for as long as 8 weeks after injection. However, transgene expression in the rAAV8-transduced muscles attenuated in the absence of an immunosuppressive regimen over the course of observation. In addition, humoral immune responses were elicited by both rAAV2 and rAAV8. mRNA levels of MyD88 and costimulating factors such as CD80, CD86, and type I interferon (interferon-β) were elevated in both rAAV2- and rAAV8-transduced DCs *in vitro*.

In our previous study, we had demonstrated extensive lymphocyte-mediated immune responses to rAAV2-*lacZ* after direct intramuscular injection into dogs, in contrast to the reported successful delivery of the same viral construct into mouse skeletal

muscle.[8] The fact that the promoter-deleted rAAV2 caused fewer cytotoxic cellular responses suggested that the massive destruction of transduced muscle cells might be the result of cellular immunity against the transgene product. In this study, there was extensive expression of β-gal in rAAV8-*lacZ*-injected canine muscles even in the absence of any immunosuppressive treatments (**Figure 1**), while the rAAV2-*lacZ*-injected muscles showed minimal β-gal expression with considerable inflammatory infiltration. If the transgene product were the main inducer of immune responses, lymphocyte activation would be correlated with transduction efficiency; however, this is not the case based on our results relating to the vector genome, mRNA expression level, and protein delivered through either rAAV2 or rAAV8 (**Figure 2**). These data suggested that the rAAV particle is associated with potent immunogenicity. Besides, β-gal expression disappeared 4 weeks after injection in the rAAV8-injected muscle as in the rAAV2-transduced muscles (**Supplementary Figure S2**). To investigate whether AAV itself has immunogenicity properties, we further characterized the immune responses caused by rAAV2 or rAAV8.

Immunohistochemical analysis revealed that the rAAV2-injected muscles showed higher rates of infiltration of $CD4^+$ and $CD8^+$ T lymphocytes in the endomysium than rAAV8-injected muscles did (**Figure 3a**). Considering the stringent immunogenicity of *lacZ* gene expression, we normalized the activity of TGF-β1 and IL-6 by lacZ expression to exclude the effect of transgene products (**Supplementary Figure S3a**). The total activity of TGF-β1 and IL-6 in the rAAV8-injected muscles was higher than that in rAAV2-injected muscles (**Supplementary Figure S3b**). As a result, rAAV2 induced a stronger cellular immune response than rAAV8 did. To investigate the humoral immune response, we quantitated neutralizing antibodies against rAAV particles in the sera of rAAV-injected dogs (**Figure 3b**). Antibodies against AAV2 and AAV8 capsids were below the detectable level before the injection and were elevated with time after the injection. Because the dogs were bred in a specific pathogen-free facility and not vaccinated, we assume that the elevation of antibody levels was not caused by anamnestic reaction.

Recently, Li *et al.*[10] reported that the AAV2 capsid can induce a cellular immune response through MHC class I antigen presentation with a cross-presentation pathway, and the effects of rAAV2 on human DCs have been described.[10,13] In contrast, other serotypes such as rAAV8 induced less T-cell activation.[11,14] Plasmacytoid DCs are critically important in innate immunity because of their unsurpassed ability to present adenoviral antigens to T-cells for the generation of primary cellular and humoral immune responses.[15–17] The response of DCs against rAAV in dogs was yet to be elucidated. We prepared bone marrow-derived DCs to investigate rAAV-mediated transduction of DCs. The difference between rAAV2 and rAAV8 in respect of the transduction rate of DCs *in vitro* was no greater than the difference in distinct β-gal expressions *in vivo* (**Figure 2,4c**). Quantitative analysis of mRNA of the transduced DCs by RT-PCR revealed that both rAAV2 and rAAV8 upregulated the expression of costimulating factors, with no significant difference between mRNA levels in rAAV2- and rAAV8-transduced cells. Therefore, both rAAV2 and rAAV8 may activate innate immunity in the context of extensive muscle transduction. Whereas AAV capsids cause immune response, transgene products may play adjuvant roles in the immunity to the AAV capsids.[18]

rAAV8 encoding the human *microdystrophin* gene was also intramuscularly injected into the skeletal muscles of $CXMD_J$ dogs. rAAV8-mediated gene expression without any immunosuppression was confirmed over a period of 8 weeks after the injection, whereas there was much less transduction with the use of rAAV2 (data not shown). rAAV8-mediated transduction was also expected to provide effective intravenous delivery.[12] In this context, the venous system is an attractive route for limb perfusion administration because it is a direct channel to multiple muscles of the limb. Moreover, veins are easier to access through the skin and there is less potential for muscle damage during injection. By using the limb perfusion method, we could reach nearly all the muscles of the lower limb, held transiently isolated by a tourniquet around the thigh. Limb perfusion administration could possibly have the potential to bypass the DC recognition caused by intramuscular injection. We intravenously injected rAAV8-*lacZ* into the hind limbs of normal dogs and rAAV8-*M3* into the hind limbs of $CXMD_J$ dogs, and obtained more extensive expression of β-gal or microdystrophin than by intramuscular injection. Interestingly, the inflammatory response was not significant in the intravenously injected muscles, although no immune suppression was attempted. We think that one reason rAAV8-*M3* resulted in better expression than rAAV8-*lacZ* is that the immunogenicity of *M3* is lower than that of *lacZ*. Although microdystrophin expression was lower at 8 weeks after the transduction with the limb perfusion, cellular infiltration was not significant.

In the future, systemic delivery of rAAV8-*microdystrophin* could ameliorate the symptoms of DMD patients. Even though portal vein injection of rAAV2-*FIX* into hemophilia B dogs produced long-term expression, a clinical study failed to demonstrate long-term expression in humans.[19,20] In advance of future clinical trials, several studies are required to confirm safety. Sequential peripheral blood monitoring showed no severe adverse events, including liver dysfunction, during 8 weeks (data not shown). We are now developing a systemic delivery strategy with a muscle-specific promoter. It is also necessary to improve vector constructs or regulate immune reaction against transgene products. Recently, Wang *et al.* reported sustained AAV6-mediated human microdystrophin expression in dystrophic dogs for 30 weeks, using combined immunosuppressive therapy of Ciclosporin, Mycophenolate Mofetil, and anti-thymocyte globulin.[9] In this study with rAAV8-*M3*, we confirmed effective transduction into dog skeletal muscle for 4 weeks without immunosuppressive therapy. However, considering the fact that not only rAAV2 but also rAAV8 induced activation of DCs *in vitro*, immunological modulation would be required for sufficient long-term expression. A novel protocol with systemic or localized immunosuppression using immunosuppressive drugs or local immunosuppression with an IFN-α or -β blockade could help avoid host immune reaction.

In summary, we achieved successful rAAV8-mediated muscle transduction in wild-type dogs as well as in dystrophic dogs by using the limb perfusion method of administration. Also, by manipulating bone marrow-derived DCs, we observed the probable contribution of antigen-presenting cells to the immune response against rAAV8-mediated gene therapy. Although the

cellular responses against rAAV8 were not significant *in vivo*, this DC activation may possibly be involved in limiting long-term transduction when the limb perfusion method is used. The limb perfusion transduction protocol with improved AAV constructs or immune modulation would further enhance rAAV8-mediated transduction strategy and lead to therapeutic benefits.

MATERIALS AND METHODS

Animals. Five- to ten-week-old male and female wild-type dogs obtained from the Beagle-based $CXMD_j$ breeding colony at the National Center of Neurology and Psychiatry (Tokyo, Japan) were used for the *lacZ* gene transduction.[9] Six- to eight-week-old $CXMD_j$ dogs were used for *microdystrophin* gene transduction. All the animals were cared for and treated in accordance with the guidelines approved by the Ethics Committee for Treatment of Laboratory Animals at National Center of Neurology and Psychiatry, where the three fundamental principles of replacement, reduction, and refinement are also considered. Dogs were not vaccinated to avoid the immune responses to vaccination.

Construction of proviral plasmid and recombinant AAV vector production. The AAV2 vector proviral plasmids harboring the *lacZ* or *luciferase* gene with a CMV promoter and SV40 late-gene polyadenylation sequence were propagated.[8] As a therapeutic gene for DMD, the human *microdystrophin* gene, *M3*, was used under the control of the CMV promoter and a bovine growth hormone polyadenylation sequence.[21] The vector genome was packaged into the AAV2 capsid or pseudotyped AAV8 capsid in HEK293 cells. A large-scale cell culture method with an active gassing system was used for transfection.[22] The vector production process involved triple transfection of a proviral plasmid, an AAV helper plasmid pAAV-RC (Stratagene, La Jolla, CA) or p5E18-VD2/8, and an adenovirus helper plasmid pHelper (Stratagene).[21] All the viral particles were purified by CsCl gradient centrifugation. The viral titers were determined by quantitative PCR using SYBR-green detection of PCR products in real time with the MyiQ single-color detection system (Bio-Rad, Hercules, CA) and the following primer sets: for AAV-*lacZ*, lacZ-Q60: forward primer 5′-TTATCAGCCGGAAAACCTACCG-3′, and reverse primer 5′-AGCCAGTTTACCCGCTCTGCTA-3′; for AAV-*microdystrophin*: forward primer 5′-CCAAAAGAAAAAGGATCCACAA-3′, and reverse primer 5′-TTCCAAATCAAACCAAGAGTCA-3′; and for AAV-*luciferase*: forward primer 5′-GATACGCTGCTTTAATGCCTTT-3′, and reverse primer 5′-GTTGCGTCAGCAAACACAGT-3′.

Direct administration of rAAVs into normal and dystrophic skeletal muscle. Experimental dogs ($n = 16$) were sedated with isoflurane by mask inhalation and intubated. Anesthesia was maintained with 2–4% isoflurane. Two milliliters of rAAV2-*lacZ* or rAAV8-*lacZ* (1×10^{11}–10^{13} vg/ml) were injected intramuscularly into the tibialis anterior muscles and 1 ml into the extensor carpi radialis muscles of the normal dogs under ultrasonographic guidance. rAAV8-*M3* (1×10^{12} vg/ml) was intramuscularly injected at a volume of 2 ml into the tibialis anterior muscles and 1 ml into the extensor carpi radialis muscles of a $CXMD_j$ dog.

Intravenous delivery of rAAVs into the limb veins of dogs. Intravenous injection was administered as described elsewhere.[12] Briefly, a blood pressure cuff was applied just above the knee of an anesthetized normal dog. A 24-gauge intravenous catheter was inserted into the lateral saphenous vein, connected to a three-way stopcock, and flushed with saline. With the blood pressure cuff inflated to over 300 mm Hg, saline (2.6 ml/kg) containing papaverine (0.44 mg/kg, Sigma-Aldrich, St Louis, MO) and heparin (16 U/kg) was injected by hand over 10 seconds. The three-way stopcock was connected to a syringe containing rAAV8-*lacZ* (1×10^{14} vg/kg, 3.8 ml/kg). The syringe was placed in a PHD 2000 syringe pump (Harvard Apparatus, Edenbridge, UK). Five minutes after the papaverine/heparin injection, the rAAV8-*lacZ* was injected at a rate of 0.6 ml/second. Two minutes after the rAAV injection, the blood pressure cuff was released and the catheter was removed. The $CXMD_j$ dogs were injected with rAAV8-*M3* using the same method.

Sampling of transduced muscles. Either the muscles of the transduced dogs were biopsied or the animals were killed at 2, 4, and 8 weeks after the injection. We sampled tibialis anterior and extensor carpi radialis muscles on both sides in the intramusculary transduced dog. In the case of the limb perfusion study, tibialis anterior or extensor digitorum longus muscle of the injected side of the leg was sampled. For biopsy and necropsy, the individual muscle was cropped tendon-to-tendon, divided into several pieces, and immediately frozen in liquid nitrogen-cooled isopentane. Two to eight blocks were sampled from the transduced muscle. We analyzed at least 30 sections from the blocks to observe the general representation.

Histological analysis. Transverse cryosections (10 μm) from the rAAV-*lacZ*-injected muscles were stained with hematoxylin and eosin or 5-bromo-4-chloro-3-indolyl-β-D-galactopyranoside.[23] Eight-micrometer-thick cryosections from the rAAV-*M3*-injected muscles were immunohistochemically stained as described.[24] Briefly, the cryosections were fixed by immersion in cold acetone at −20 °C. Fixed frozen sections were blocked in 5% goat serum in phosphate-buffered saline at room temperature and incubated with mouse monoclonal anti-dystrophin C-terminal antibody (NCL-dys2, Novocastra, Newcastle upon Tyne, UK). The signal was visualized with an Alexa 568-conjugated anti-mouse IgG. Fluorescent signals were observed using a confocal laser scanning microscope (Leica TCS SP, Leica, Heidelberg, Germany). Immunohistochemical analyses were performed with mouse monoclonal antibodies against canine CD4 (CA13.1E4, Serotec, Oxford, UK), canine CD8a (CA9. JD3, Serotec), and double-stained with rabbit polyclonal antibody against α-sarcoglycan.[25] The signal was visualized with an Alexa 568-conjugated anti-mouse IgG, and 488-conjugated anti-rabbit IgG.

Detection of AAV genomes. Total DNA was extracted from muscle cryosections. Cryosections were homogenized using a Multi-beads shocker (Yasui Kikai, Osaka, Japan), and extracted using a Wizard SV Genomic DNA purification system (Promega, Madison, WI). The rAAV genome was detected by relative quantitative PCR using SYBR-green detection of PCR products in real time with a primer set of *lacZ*-Q60. For an internal control, forward primer, 5′-GAACACGCGTTAATAAGGCAATCA-3′, and reverse primer, 5′-CTGACATTCATCGCATCTTTGACA-3′, directed to an ultra-conserved region, were used.[26]

Real-time RT-PCR. Total RNA was isolated from cryosections using a Multi-beads shocker (Yasui Kikai), and RNeasy Fibrous Tissue Mini kit (Qiagen, Hilden, Germany), and first-strand cDNA was synthesized using a QuantiTect Reverse Transcription kit (Qiagen). mRNA was detected using primer sets of lacZ-Q60, forward primer 5′-TGATGGCTA CTGCTTTCCCTAC-3′ and reverse primer 5′-GAGATTTTGCCGA GGATGTACT-3′ for IL-6, and forward primer 5′-CAAGGATCTGGGC TGGAAGTGGA-3′ and reverse primer, 5′-CCAGGACCTTGCTGTA CTGCGGT-3′ for TGF-β1. For an internal control, a primer set of 18S rRNA (Ambion, Foster City, CA) was used.

Western blot analysis. Muscle cryosections were homogenized with four volumes of sample buffer (10% SDS, 70 mmol/l Tris-HCl, 10 mmol/l EDTA, and 5% β-mercaptoethanol). The samples were boiled for 5 minutes and centrifuged at 14,500 rpm for 15 minutes. Protein samples (30 μg per lane) were electrophoresed on a 7.5% polyacrylamide gel (Bio-Rad). The membranes were incubated with a 1:1,000 dilution of the primary antibody for detecting 120 kDa lacZ protein (rabbit anti-β-galactosidase IgG fraction, Molecular Probes, Eugene, OR) or 42 kDa α-actin (mouse anti α-sarcomeric actin IgM, Sigma-Aldrich). Anti-rabbit IgG peroxidase F(ab′)